NiSi THIN FILM FABRICATION BY PULSED LASER DEPOSITION

Zang Hui

A THESIS SUBMITTED FOR THE

DEGREE OF MASTER OF SCIENCE

NATIONAL UNIVERSITY OF SINGAPORE

2006

Acknowledgement

I would like to express deep gratitude to my project supervisor Associate Professor Shen Zexiang for his patient guidance and encouragement throughout the course of this project. I would also like to extent sincere thanks to Dr Zhu Yong for his support in this research work, and Mr Ni Zhenhua for his guidance in usage of the micro-Raman spectroscopy system.

Table of Content

Summary

In this thesis, we report NiSi film fabrication by the application of Pulsed Laser Deposition (PLD) using Ni and Si targets with the proportion of 1:1. This technique minimizes Si consumption from Si wafer substrate. After annealing, the thin film characteristics of the NiSi thin films was investigated using Micro-Raman spectroscopy (μRS), X-Ray Diffraction (XRD), and Atomic Force Microscopy (AFM). Phase identification was carried out by μRS and XRD. XRD also shows that NiSi thin film prepared with Ni/Si target possessed of preferred orientation of NiSi（001）on Si (001) substrate. The texture properties of the thin films were strongly affected by annealing temperature and the Ni/Si ratio of as-deposited samples. AFM also shows that the NiSi thin films prepared by Ni/Si target gave smoother surface compared to those prepared by pure Ni target.

Chapter 1

Introduction of NiSi application in CMOS device fabrication

1.1 Metal Silicide application in CMOS device fabrication

Metal-oxide-semiconductor field-effect-transistor (MOSFET) is the basic building block for the absolute majority of today's electronic systems. The focus of this research is on the use of metal silicides for MOSFET devices. A cross section of two modern MOSFETs placed side-by-side is shown schematically in Figure 1.1, with metal silicide layers at the three electrode terminals, namely gate, source, and drain, of each transistor. The silicide layer is formed simultaneously in all six electrode areas. The two transistors are of opposite polarity, with one n-channel MOSFET (n MOSFET) built directly on the p-type substrate, and one p-channel MOSFET (p MOSFET) built inside the n-well. Constructed simultaneously on the same substrate, the two transistors are usually connected in series between the power supply terminals in an electronic circuit to minimize standby power dissipation, that is, the complementary MOS (CMOS) technology [1.1].

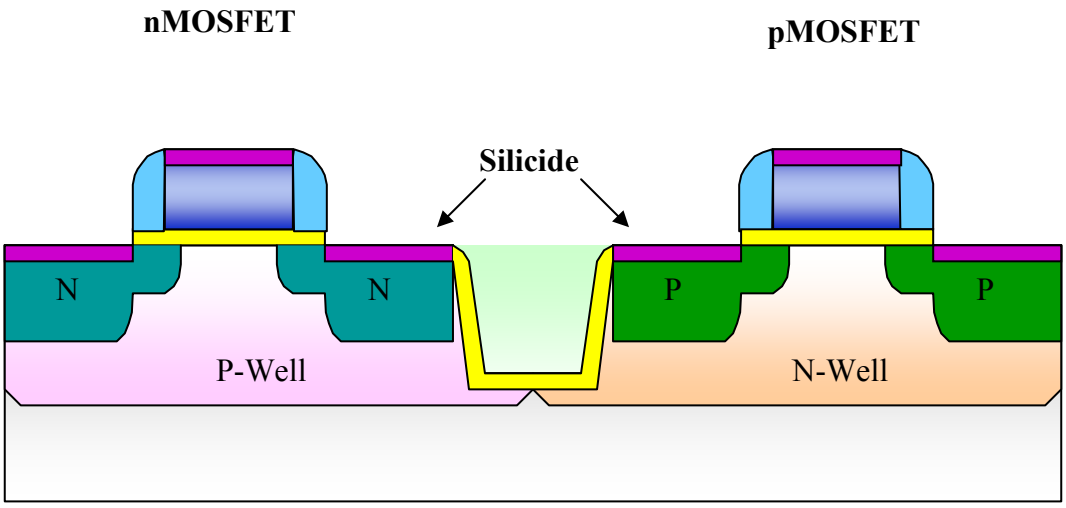

Figure 1.1 Cross section of modern CMOS transistors with an n-channel MOSFET (n MOSFET) and a p-channel MOSFET (p MOSFET)

A general self aligned silicidation (Salicide) process is summarized in Figure 1.2, using the formation of NiSi as an example. It starts with Ni metal layer deposited over the entire surface of a wafer substrate, where various structures are already defined and different materials, including Si and SiO_2, are present. After annealing, the deposited Ni only reacts with Si in the areas where Si is in contact with the metal. The metal does not react with the surrounding dielectric materials such as SiO_2. Selective removal of the unreacted metal on top of SiO_2 can be realized with wet chemicals. The salicide process has been very successful due to its great process simplicity. NiSi has attracted a great deal of attention due to its excellent electrical properties. The latest developments point to a converging effort to incorporate NiSi in future MOS devices.

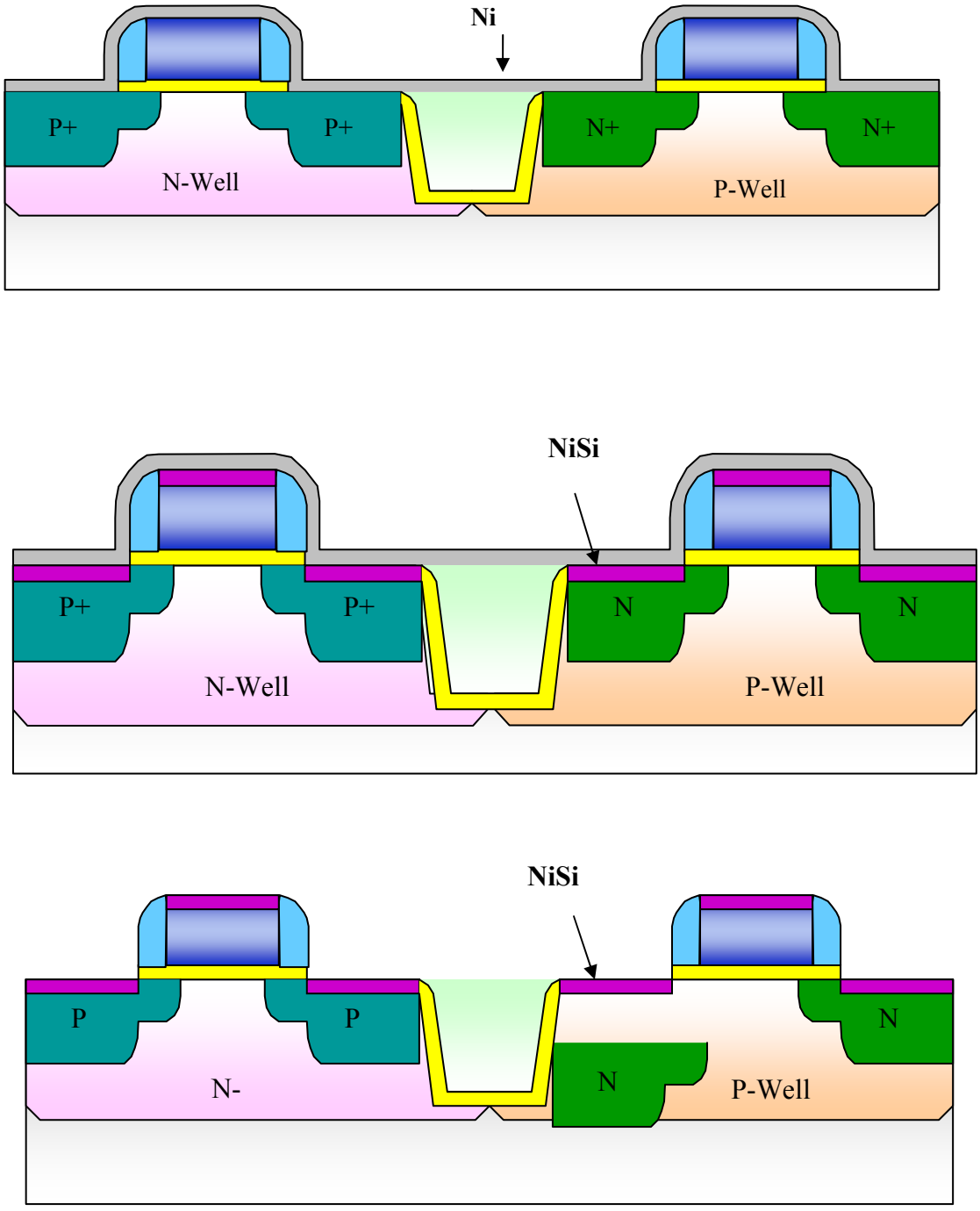

Figure 1.2 A schematic NiSi formation process.

As the electrical contact between metal and semiconductor, silicide resistivity should be scaled according to the International Technology Roadmap for Semiconductors (ITRS) in order to deliver MOSFETs with the desired performance shown in Figure 1.3.

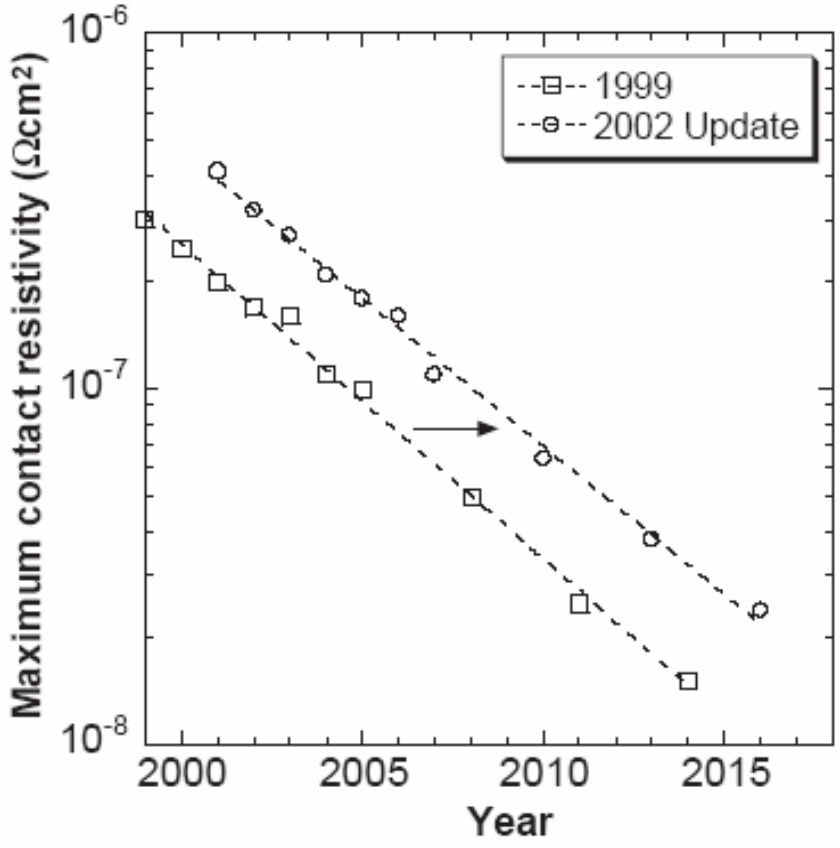

Figure 1.3 Maximum contact resistivity as predicted in ITRS 1999 and 2002 update [1.1].

NiSi for contact metallization shows a number of technological advantages, (1) low formation temperature, (2) the lowest achievable specific resistivity, (3) smooth silicide/Si interface, and (4) low Si consumption [1.2]. However, NiSi has not been considered a serious candidate until recent, mainly due to its low

morphological stability and the risk of the formation of the high-resistivity $NiSi_2$. A greatly enhanced phase stability of NiSi by alloying Ni with Pt has been reported [1.3].

For CMOS technologies beyond the 90 nm node, Si consumption from Si wafer due to silicide formation should be minimized further. Until now, this has yet to be addressed effectively. Here we report NiSi film fabrication using pulsed laser deposition (PLD), which is a large step to fit this requirement.

1.2 References

[1.1] S. L. Zhang and M. Ostling, *Crit. Rev. Solid State Mater. Sci.*, **28**, 1 (2003).

[1.2] F. F. Zhao, S. Y. Chen, Z. X. Shen, X. S. Gao, J. Z. Zheng, A. K. See, and L. H. Chan, *J. Vac. Sci. Technol. B*, **21**, 862 (2003).

[1.3] P. S. Lee, D. Mangelinck, K. L. Pey, Z. X. Shen, J. Ding, T. Osipowicz, and A. See, *Electrochem. Solid-State Lett.*, **3**, 153 (2000).

Chapter 2

Raman Classical Theory

2.1 Introduction

The Raman effect was theoretically predicted in 1923 by Smekal. He predicted that molecules could scatter light inelastically, and suggested that molecular polarization changes as particular vibration. Not long after that in 1928, Professor Chandrasekhara Venkata Raman in India found that if monochromatic light passes through a transparent substance, new weak lines of different frequencies appear in the spectrum in addition to the excitation frequency. This radiation effect gained him the 1930 Physics Nobel Prize [2.1, 2.2].

After the availability of laser, which provides strong, coherent monochromatic light in a wide wavelength range, Raman spectroscopy was used as an important analytical technique for material identification [2.3]. The Stokes and anti-Stokes shift uniquely identify the molecule and its quantum state. Therefore Raman becomes chemical "fingerprint" of material [2.4]. Compared to other characterization equipments, Raman spectroscopy is straightforward, non-destructive, and requires no sample preparation. In the past few years, there was significant development in the micro-Raman spectroscopic technique, and nowadays it is widely utilized in academy and industry.

2.2 Basic Definitions

Raman scattering is a process resulting from the interaction of radiation with material. An exciting light beam irradiates one material will lead to additional light with new frequency, which is called Raman scattering. Raman scattering by molecules is composed of two parts: a) the elastic Rayleigh scattering with no change in frequency ("Rayleigh scattering") [2.5, 2.6] and b) the inelastic Raman scattering ($\nu_0 \pm \nu_m$), which carries with the information of vibrational and rotational energy levels of the molecules [2.6,2.7].

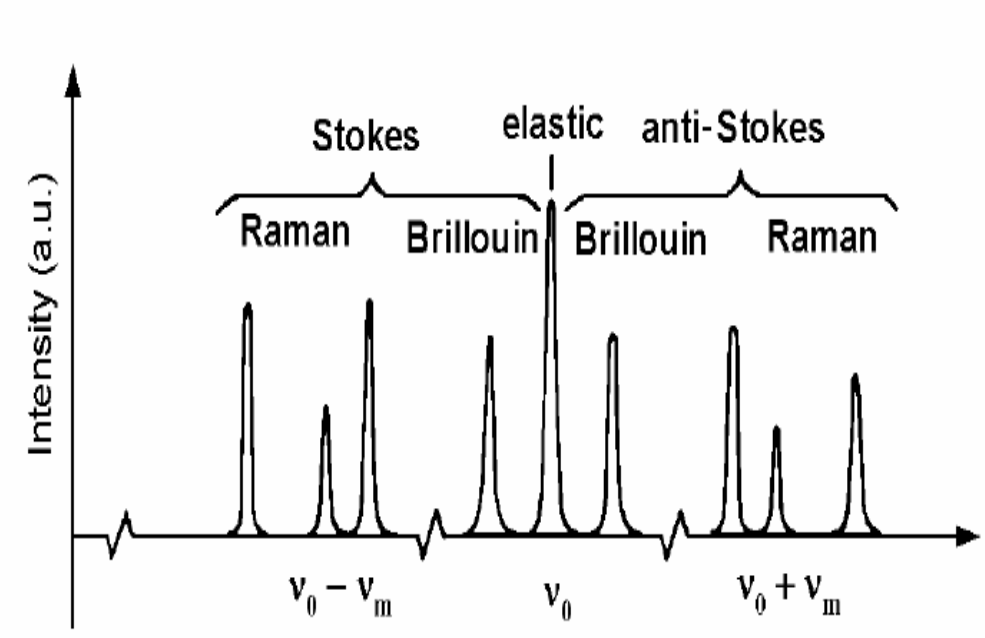

Figure 2.1 Schematic spectrum of scattered light [2.6]

The Brillouin component shown in Fig 2.1, is the scattering by sound waves. Typical shifts are approximately within $1cm^{-1}$. The Raman component lies at higher shifts, normally larger than $10cm^{-1}$ and are often of order $100\text{-}1000cm^{-1}$. Raman scattering in the low frequency side of the Raileigh line is called Stokes Lines. The opposite counterpart is Anti-Stokes lines, as shown in Fig 2.1. The basic mechanisms for Brillouin and Raman scattering are essentially the same, but the experimental techniques are different.

2.3 Basic Theory

In classical theory, Raman scattering is explained as follows: The time dependence of the electric field (E) of the electromagnetic wave (laser beam) can be written as,

$$E = E_0 \cos 2\pi\nu_0 t \tag{2.1}$$

where E_0 is the amplitude and t is time. If a diatomic molecule is irradiated by this light, the dipole moment P given by

$$p = \alpha E = \alpha E_0 \cos 2\pi\nu_0 t \tag{2.2}$$

which is induced [2.7]. Here α is a proportionality constant and is called the polarizability. If the molecule is vibrating with a frequency ν_m, the nuclear displacement q is written as

$$q = q_0 \cos 2\pi\nu_m t \tag{2.3}$$

where q_0 is the vibrational amplitude. Assuming the vibrational amplitude is small, the polarizability can be expressed as:

$$\alpha = \alpha_0 + \left(\frac{\partial\alpha}{\partial q}\right)_0 q + \ldots \tag{2.4}$$

Here, α_0 is the polarizability at the equilibrium position, and $\left(\frac{\partial\alpha}{\partial q}\right)_0$ is the rate of change of α with respect to the change in q, evaluated at the equilibrium position [2.7].

Combining Eqs. 2.2-2.4, we have

$$
\begin{aligned}
p &= \alpha E_0 \cos 2\pi\nu_0 t \\
&= \alpha_0 E_0 \cos 2\pi\nu_0 t + \left(\frac{\partial\alpha}{\partial q}\right)_0 q E_0 \cos 2\pi\nu_0 t \\
&= \alpha_0 E_0 \cos 2\pi\nu_0 t + \left(\frac{\partial\alpha}{\partial q}\right)_0 q_0 E_0 \cos 2\pi\nu_0 t \cos 2\pi\nu_m t \\
&= \alpha_0 E_0 \cos 2\pi\nu_0 t + \frac{1}{2}\left(\frac{\partial\alpha}{\partial q}\right)_0 q_0 E_0 [\cos\{2\pi(\nu_0 + \nu_m)t\} + \cos 2\pi(\nu_0 - \nu_m)t]
\end{aligned}
\tag{2.5}
$$

The first term in Eq.2.5 describes Rayleigh scattering and the remaining terms describe the Raman scattering of frequency $\nu_0+\nu_m$ (anti-Stokes) and $\nu_0-\nu_m$ (Stokes). If $(\frac{\partial\alpha}{\partial q})_0$ is zero, the vibration is not Raman-active. Namely, to be Raman-active, the rate of change of polarizability (α) with the vibration must not be zero [2.4, 2.7].

In actual molecules, both *P* and *E* are vectors consisting of three components in the *x*, *y* and *z* direction. Consequently, Eq. 2.2 must be written as

$$
\begin{aligned}
P_x &= \alpha_{xx}E_x + \alpha_{xy}E_y + \alpha_{xz}E_z \\
P_y &= \alpha_{yx}E_x + \alpha_{yy}E_y + \alpha_{yz}E_z \\
P_z &= \alpha_{zx}E_x + \alpha_{zy}E_y + \alpha_{zz}E_z
\end{aligned}
\tag{2.6}
$$

In matrix form, this is written as

$$
\begin{bmatrix} P_x \\ P_y \\ P_z \end{bmatrix} = \begin{bmatrix} \alpha_{xx} & \alpha_{xy} & \alpha_{xz} \\ \alpha_{yx} & \alpha_{yy} & \alpha_{yz} \\ \alpha_{zx} & \alpha_{zy} & \alpha_{zz} \end{bmatrix} \begin{bmatrix} E_x \\ E_y \\ E_z \end{bmatrix} \tag{2.7}
$$

The first matrix on the right-hand side is called the polarizability tensor. In normal Raman scattering, this tensor is symmetric [2.4, 2.7].

$\alpha_{xy}=\alpha_{yx,}$ $\alpha_{xz}=\alpha_{zx}$ and $\alpha_{yz}=\alpha_{zy}$. (2.8)

Raman scattering induced by the vibrations of polyatomic molecules has been introduced classically. Other Raman scattering phenomena, particularly the rotational and electronic Raman effect, are more easily understood as quantum mechanical phenomena [2.8].

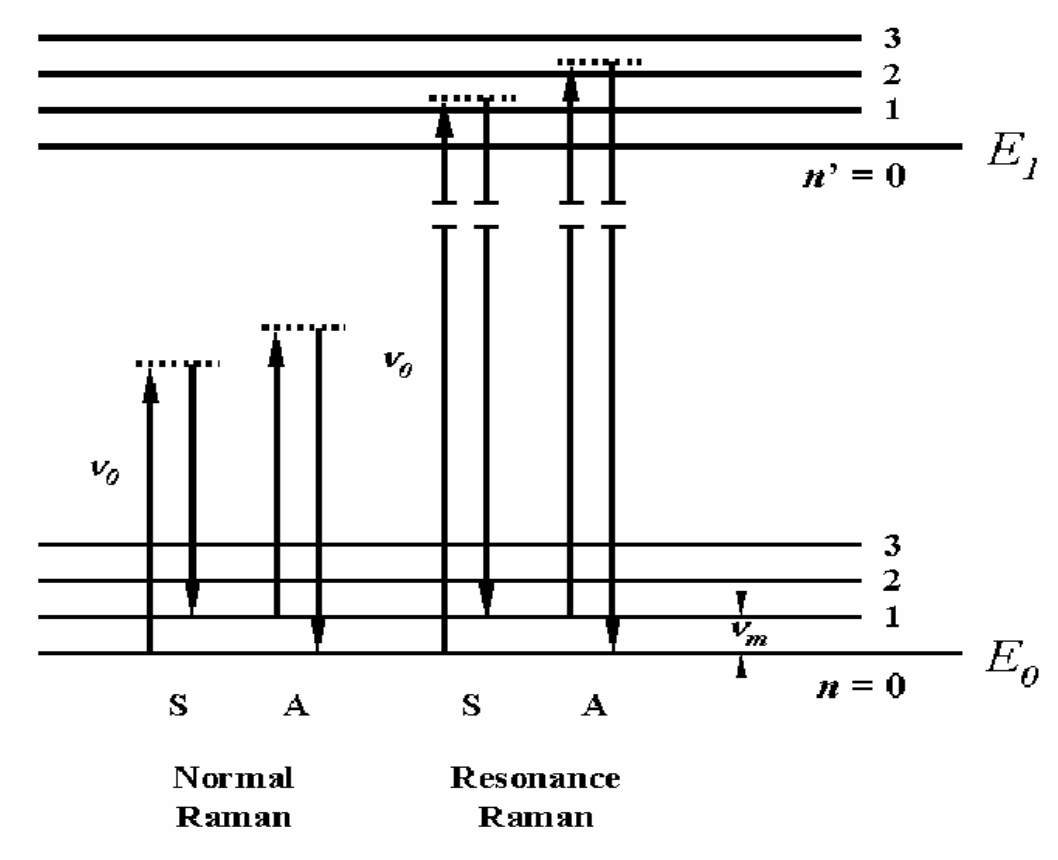

Figure 2.2 Comparison of energy levels for normal Raman and resonance Raman. [2.7]

A schematic diagram demonstrating the quantum theory of Raman scattering is shown in Fig 2.2. The quantum theory of spectroscopic processes should treat the exciting light and molecule together as a complete system, and explain how

energy may be transferred between the exciting light and the molecule as a result of their interaction.

The vibrational energy of a molecule is quantized according to the relationship:

$$E_n = h\nu(n + 1/2) \tag{2.10}$$

where h is Planck's constant, and n is the vibrational quantum number and has values of 0, 1, 2, … . If a molecule is placed in an electromagnetic field (light), a transfer of energy from the field to the molecule will occur when Bohr's frequency condition is satisfied:

$$\Delta E = h\nu \tag{2.11}$$

where ΔE is the difference in energy between two quantized states, and ν is the frequency of the light. Suppose that

$$\Delta E = E_1 - E_0 \tag{2.12}$$

where E_1 and E_0 are the energies of the excited and ground states respectively. Then the molecule "absorbs" ΔE when it is excited from E_0 to E_1 and "emits" ΔE when it reverts from E_1 to E_0.

In normal Raman spectroscopy, the excitation line (ν_0) is chosen so that its energy is far below the first electronic excited state. The dotted line indicates a "virtual state" to distinguish it from the real excited state. At room temperature there will be much more molecules in the ground vibrational state than in the higher vibrational states, and therefore the incoming light is more likely to interact with a molecule in the ground state and excite it to a higher vibrational state, giving rise to a Stokes line. Molecules lose energy and fall back to the ground state, giving

rise to an anti-Stokes line, only if incoming light collides with a molecule in one of the higher energy states. [2.6]. Therefore the intensity of Stokes line is much higher than that of Anti-Stokes line, As such, Raman analysis typically only involves the studying of Stokes Peaks.

Resonance Raman (RR) scattering occurs when the exciting line is chosen to E_1, so that its energy intercepts the manifold of an electronic excited state. In the gaseous phase, this tends to cause resonance fluorescence since the rotational-vibrational levels are discrete. However, in the liquid and solid states, vibrational levels are broadened to produce a continuum due to molecular collisions and/or intermolecular interactions [2.4, 2.7]. Excitation of these continua produces RR spectra, which shows extremely strong enhancement of Raman bands originating in this particular electronic transition [2.7]. So RR can be achieved by changing the laser wavelength, and a stronger Raman signal could be obtained.

2.5 References

[2.1] G. M. Begun, *Fundamental theory and techniques of Raman spectroscopy*, Oak Ridge, Tenn: Oak Ridge National Laboratory, 1981, pp. 1-2.

[2.2] V. A. Afanasiev, G. E. Zaikov, *Physical methods in chemistry*, edited by Vitaly A. Afanasiev and Gennady E. Zaikov, New York: Nova Science, 1992, pp. 87-88.

[2.3] L. Qin, *Raman Study of Ge/Si QDs Nano Structure Under High Hydrostatic Pressure*, Thesis (Ph.D.)--Dept. of Physics, Faculty of Science, National University of Singapore, 2002.

[2.4] M. Cardona, *Light scattering in solids*, edited by M. Cardona, Berlin: Springer-Verlag, 1975, pp.1-2.

[2.5] K. Nakamoto, *Infrared and Raman Spectra of Inorganic and Coordination Compounds*, New York: John Wiley & Sons, Inc., 1997, pp.1-33.

[2.6] W. Hayes, R. Loudon. *Scattering of Light by Crystals*, New York: Wiley, 1978, pp.3-6.

[2.7] J. R. Ferraro, K. Nakamoto, *Introductory Raman Spectroscopy*, Boston: Academic Press, 1994, pp.15-23.

[2.8] T. R. Gilson, P. J. Hendra, *Laser Raman Spectroscopy: a Survey of Interest Primarily to Chemists, and Containing a Comprehensive Discussion of Experiments on Crystals*, London: Chichester, Wiley-Interscience, 1970, pp.9-10.

Chapter 3

NiSi thin film fabrication by Pulsed Laser Deposition (PLD)

3.1 Pulsed Laser Deposition

Introduction of pulsed laser deposition

Pulsed laser deposition is a technique for fabricating thin films. Fig.3.1 shows the schematic diagram of a Pulsed Laser Deposition system. The PLD method of thin film growth involves evaporation of a solid target in a high vacuum chamber by means of short and high-energy laser pulses. In a typical PLD process, a ceramic target is placed in the sample chamber [3.1].

In laser ablation, high-power laser pulses are used to evaporate target surface so that the stoichiometry of the material is preserved in the interaction. Then a supersonic jet of particles is ejected from the target surface. The plume expands away from the target. The ablated species condense on the substrate placed opposite to the target.

The film area is determined by the dimension of the plume, and it is typically 1cm². The area can be increased by scanning the laser spot across the target or the plume across the substrate by moving the substrate relative to the plume, or by changing the target-substrate distance [3.2].

The targets used in PLD are small compared with that for sputtering techniques. It is very easy to produce multi-layered films of different materials by sequential ablation of assorted targets. The most important feature of PLD is that the stoichiometry of the target can be retained in the deposited films. Due to the high heating rate of the ablated materials, laser deposition of crystalline film demands a much lower substrate temperature than other film growth techniques. For this reason the semiconductor and the underlying integrated circuit are exempted from thermal degradation.

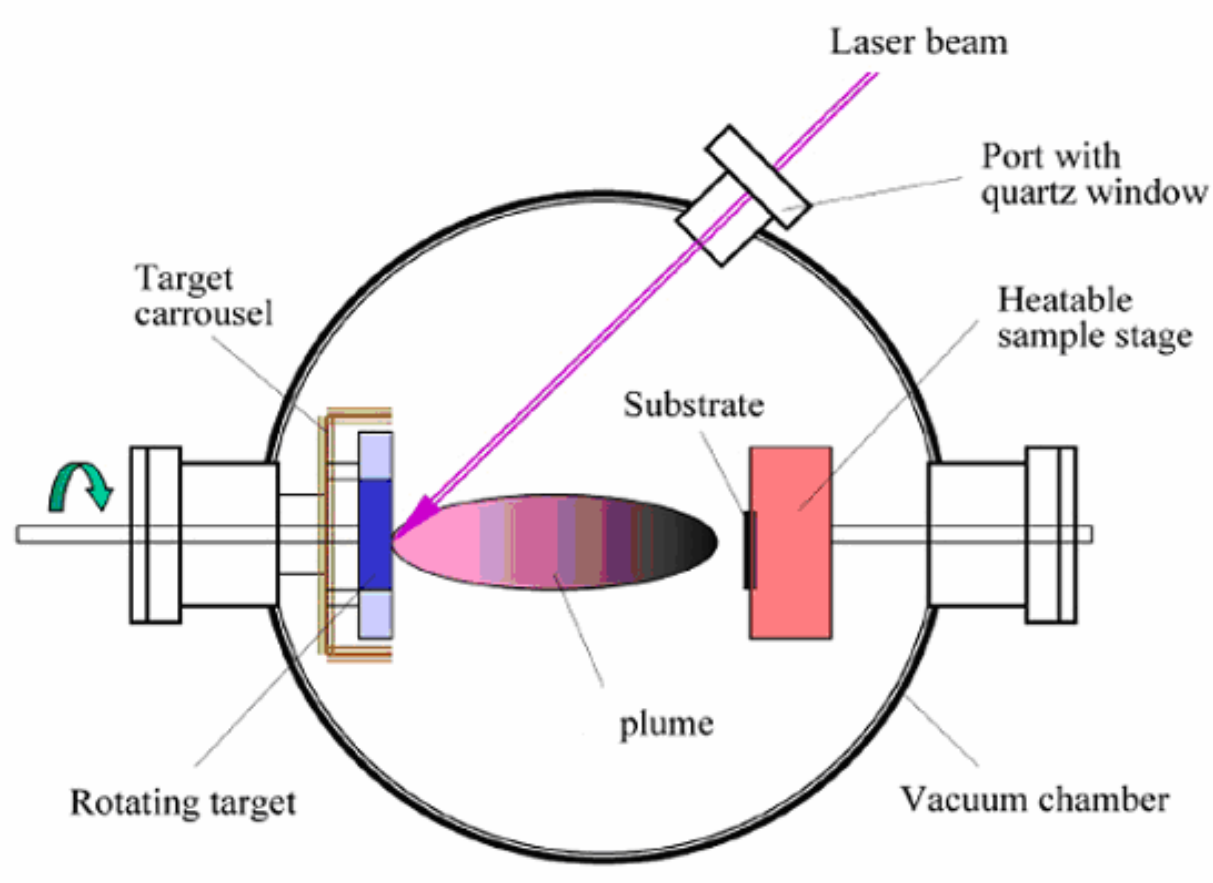

Figure 3.1, Schematic diagram of a Pulsed Laser Deposition system

Advantages of PLD method

PLD is conceptually simple and versatile. Many materials can be deposited in a wide variety of gas ambient over a broad range of gas pressure. It is also cost-effective since one laser can serve many sample chambers. It is also fast. Samples can be grown reliably in 10 to 15 minutes.

PLD enables the congruent transfer of materials. Films have the same composition as the target when the focused laser energy density is chosen properly. Deposition is from an energetic plasma beam. Growth of multilayered epitaxial heterostructures can be accomplished with the use of multiple or multi-element targets. The substrate temperature can be independently set [3.3].

3.2 Rapid thermal processor

Introduction of Rapid thermal processor

Rapid thermal processing (RTP) is a fast-ramp thermal processing capability that can be used to heat a wafer from room temperature to 1100^{o}C in matter of seconds. Typical ramp rates used in RTP are 50-75^{o}C/sec. Recently, RTP systems have boasted controlled ramp rate exceeding 300^{o}C/sec. In RTP, annealing is carried out in a single-wafer chamber. During processing, a Si wafer is placed in the middle of the chamber surrounded by quartz walls, see Fig 3.2. The wafer is seated on three quartz pins protruding from a quartz susceptor, so as to minimize

the physical contact between the wafer and the susceptor. This helps to achieve a uniform heat distribution when the Si wafer is being heated up. Two lamps banks, each with a set of linearly-shaped lamps, are used for wafer heating. To improve the heating efficiency, reflectors are placed outside the quartz chamber. Quartz parts are used in order to minimize the total mass for heating, because quartz poorly absorbs radiated energies coming from the lamps [1.1].

The wafer temperature is detected with a pyrometer under the wafer. By comparing the set-point temperature and the pyrometer readout, the electrical power of heating lamps is regulated to yield the set-point temperature. Because the pyrometer readout depends strongly on the emissivity of the Si wafer, the smoothness of the Si wafer surface is very important. The temperature can also be detected by a thermal couple. For wafer temperature, it is very important to analyze wafer-heating mechanisms as well as to identify factors which affect the heating process. In general, accurate modeling and precise control of the wafer temperature are challenging tasks because of the fact that the emissivity of Si is not only wavelength and temperature dependent, but also sensitive to surface roughness and doping concentration. Temperature non-uniformity across the wafer can then build up due to the local differences in heat absorption as well as finite thermal conductivity within the substrate [1.1].

-

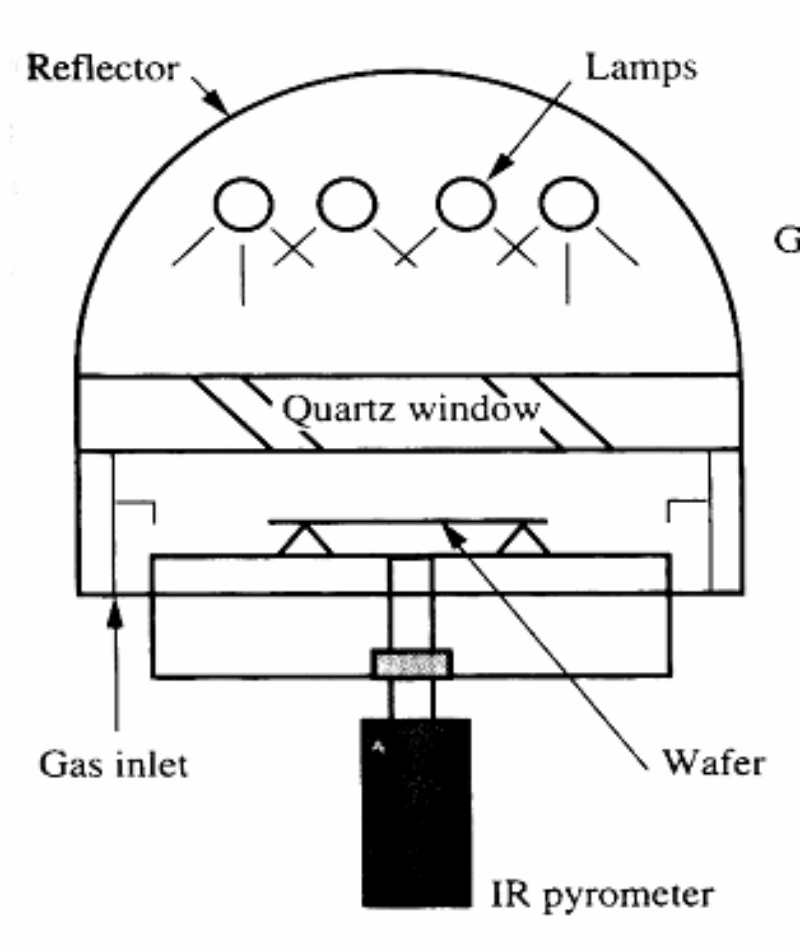

Figure 3.2 schematic diagram of a RTP chamber

Advantages of RTP

By using RTP, the thermal budget is reduced. As a result of the rapid ramp rates in RTP system, the wafer experiences a smaller thermal exposure than a wafer in a batch furnace. High temperature and short time anneals also reduce the transient-

enhanced diffusion effects (TED). This is typically unachievable in furnaces, making RTP an ideal tool for forming shallow junctions. RTP systems are small and symmetrically designed, allowing more uniform process gas distribution in the RTP chamber as compared to that of a furnace. RTP processes involve less contamination than furnace due to its cold wall nature.

3.3 Experimental

NiSi thin films were prepared by the PLD technique. A Nd: YAG pulsed laser (Spectra-Physics, GCR-170) beam of 355nm wavelength (by third harmonic generation) and 10Hz pulsed frequency was used to ablate the target in a high vacuum chamber. With Q switching, the laser pulse width was generally less then 10ns and its power could reach 10^8 W. The laser spot size could be focused to less than 1 mm in diameter on the target. Both Si (99.99%) and pure Ni (99.99%) targets were used in our experiment. The Si (001) wafer was glued onto the surface of the Ni target. During the PLD process, the centre of the Ni-Si target assembly was set to rotate slowly around its central axis and the laser beam vaporized the two component materials alternately. The Si wafer substrate was cleaned by diluted Hydrofluoric Acid (HF) to remove the native oxide and then by ultrasonic bath. The base pressure of the vacuum chamber was 4×10^{-6} torr. The laser deposition was carried out for 60 min, with the target rotating at a speed of about 3 RPM. The thin film (measured by profile-meter) is about 70nm in

thickness. The stoichiometry of the as-deposited Ni_xSi_y films can be controlled easily in PLD system. The samples whose Ni/Si ratio are 1:1(Group A) and 2:1 (Group B) were annealed at 500, 600, 700^oC for 60 seconds by RTP to obtain the metastable and stable phase of salicides. For good sample-to-sample uniformity, each group of samples was cut from the same as-deposited sample prior to the annealing splits. For comparison, pure Ni thin film of about 40 nm (Group C) was also prepared. After annealing at 500^oC or 600^oC, it forms 70-80nm NiSi which is comparable to Group A and Group C samples.

3.4 References

[3.1] Douglas H. Lowndes, D. B. Geohegan, A. A. Puretzky, D. P. Norton, and C. M. Rouleau, *Science*, **273**, 898 (1996).

[3.2] F. Roozeboom and N. Parek, *J. Vac. Sci. Technol. B*, **8**, 1249 (1990).

[3.3] R. Kakoschke, *Mater. Res. Soc. Symp. Proc.*, **224**, 159 (1991).

[3.4] Byung-Jin Cho, Peter Vandenabeele, and Karen Maex, *IEEE Trans. on Semicond. Manuf.*, **7**, 345 (1994).

Chapter 4

Thin Film Characterizations by Micro-Raman Spectroscopy and Atomic Force Microscopy

4.1 Micro-Raman spectroscopy instrumentation

Micro-Raman spectroscopy (μRS) normally consists of four basic components: (1) a intense monochromatic light source, (2) a CCD detector, (3) an amplification system, (4) computer system for instrument control, data acquisition and processing.

The basic principle of Raman microscopy is as the following. The sample to be examined is placed on the sample stage and is viewed using an incident white light either on the TV monitor connected to the closed circuit television viewing system (CCTV) or through the eyepieces. The sample area of interest is located and irradiated by a visible laser beam. The light source emits a directional polarized beam which is directed onto a semi-reflecting mirror (beam splitter) in an optical microscope. A portion of incident laser radiation is reflected downwards through the microscope objective lens which serves to focus the laser beam to a diffraction-limited spot, while the other portion is transmitted through the beam splitter. The reflection and transmission characteristics of the beam splitter are determined by the dielectric coating used. The scattering radiation collected is then directed and focused by coupling optics onto the entrance slit of the grating spectrometer, which act as a tunable filter. The output of the grating spectrometer

is focused onto the CCD detector and the resultant signal is recorded in the microcomputer which is used to control the spectrograph and detector.

Experimental

The micro-Raman system that we used is a Jobin-Yvon T6400 Raman System. This is a triple grating spectrograph/scanning spectrometer system (Fig. 4.1). The Raman spectra were recorded in the backscattering geometry at room temperature using the 488nm (2.541eV) line from a Spectra Physics Stabilite 2017 argon ion laser.

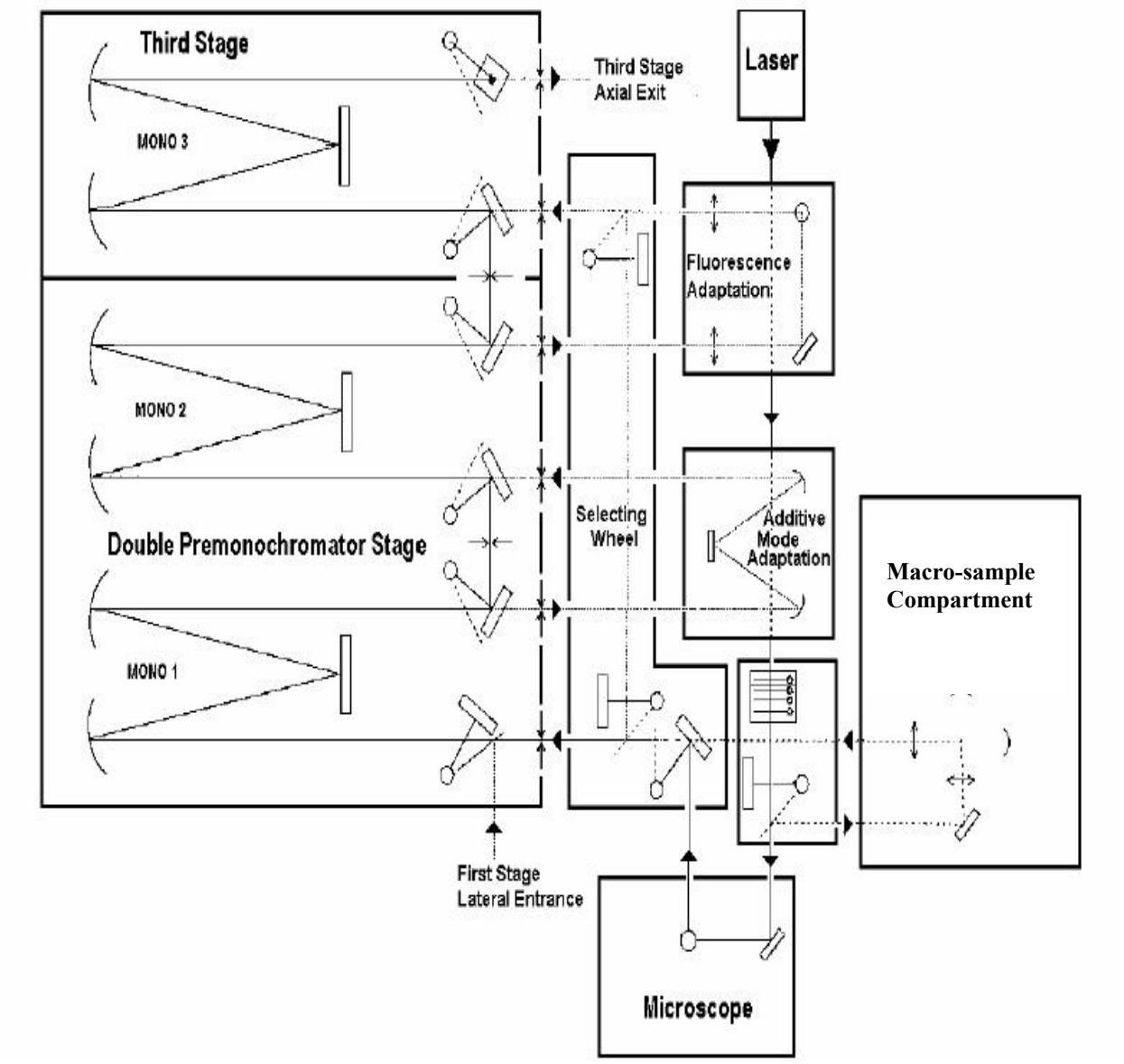

Figure 4.1 Optical functional diagram of the Jobin-Yvon T64000 Raman system

4.2 Raman study of NiSi

NiSi is a suggested candidate for future integrated circuit generations due to its linewidth-independent, low-resistivity, low process temperature, one-step annealing and low silicon consumption. In this section, we will discuss the study of NiSi thin films by micro-Raman spectroscopy. Micro-Raman spectroscopy provides information on the vibrational properties of a material. It serves as a material fingerprint and allows analysis of its vibrational modes and interatomic forces [4.1]. Some conventional methods show limitations in current salicide characterization, especially when the film thickness and device dimension continue to shrink. Micro-Raman spectroscopy is a versatile technique for the study of thin films. By detecting molecular vibrations determined by crystal structure and chemical bonding as well as the masses of the constituent atoms or ions, it is unique in chemical identification, contaminant analysis, and phase transition and stability studies [4.1]. Compared with other traditional characterization techniques, μRS possesses a number of advantages. It is fast, non-contact and nondestructive; Furthermore, no special sample preparation is required. It also possesses a high spatial resolution of about 0.5 μm, governed by the theoretical diffraction limit.

The micro-Raman spectroscopy technique has been applied in the characterization of Ni silicides primarily for the purpose of identifying the Ni_2Si, NiSi, and $NiSi_2$ phases. The Raman spectrum is related to the crystallographic structure of the

compounds. Hence, the change in Raman spectra is attributed to the phase change of Ni silicide.

As shown in Fig 4.2, in the Ni–Si binary sample, Ni diffuses into the silicon substrate to form high resistivity Ni_2Si at about 200°C. The transformation of the preferred low resistivity phase NiSi starts at 400°C. Another high resistivity phase $NiSi_2$, which should be avoided in device fabrication, nucleates at above 700 °C.

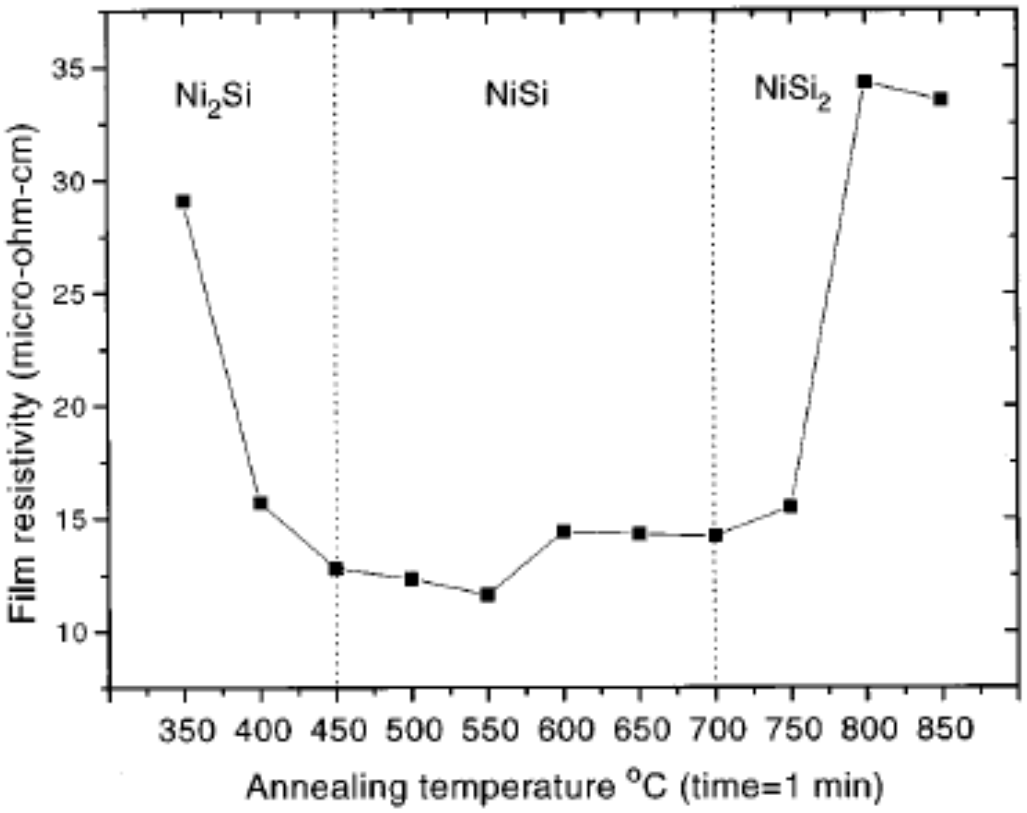

Fig 4.2 Ni silicide resistivity as a function of annealing temperature for a one minute anneal [1.1].

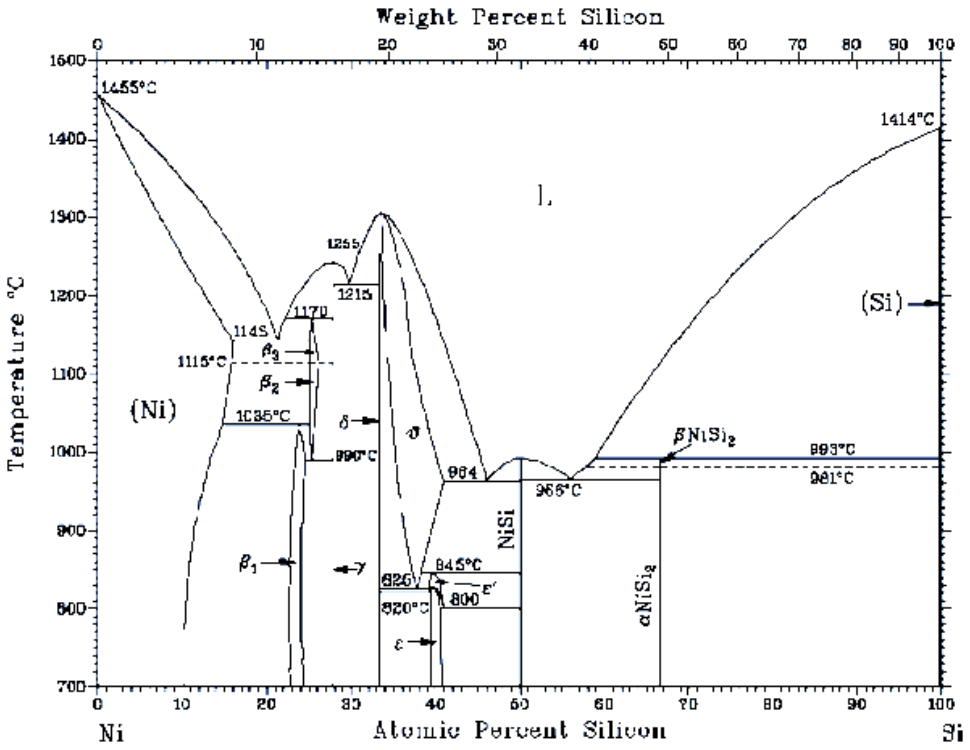

Figure 4.3 Binary phase diagram for Ni-Si [1.1]

Ni	$NiSi_3$	Cubic
	Ni_2Si	Orthorhombic
	NiSi	Orthorhombic
	$NiSi_2$	Cubic
Si	Si	Cubic

Table 4.1 Ni silicides crystal structure

The silicide phases that may form during solid-state interactions between Ni thin film and Si substrates can be found in Fig 4.3, the phase diagram for the Ni-Si

binary system. Stable phases are presented with their composition domains varying with temperature at standard atmospheric pressure. β_1, β_2 and β_3 phase were Ni_3Si of different Si percentage or different prototype. δ is Ni_2Si. Every phase of Ni Silicide has different crystal structure as shown in Table 4.1:

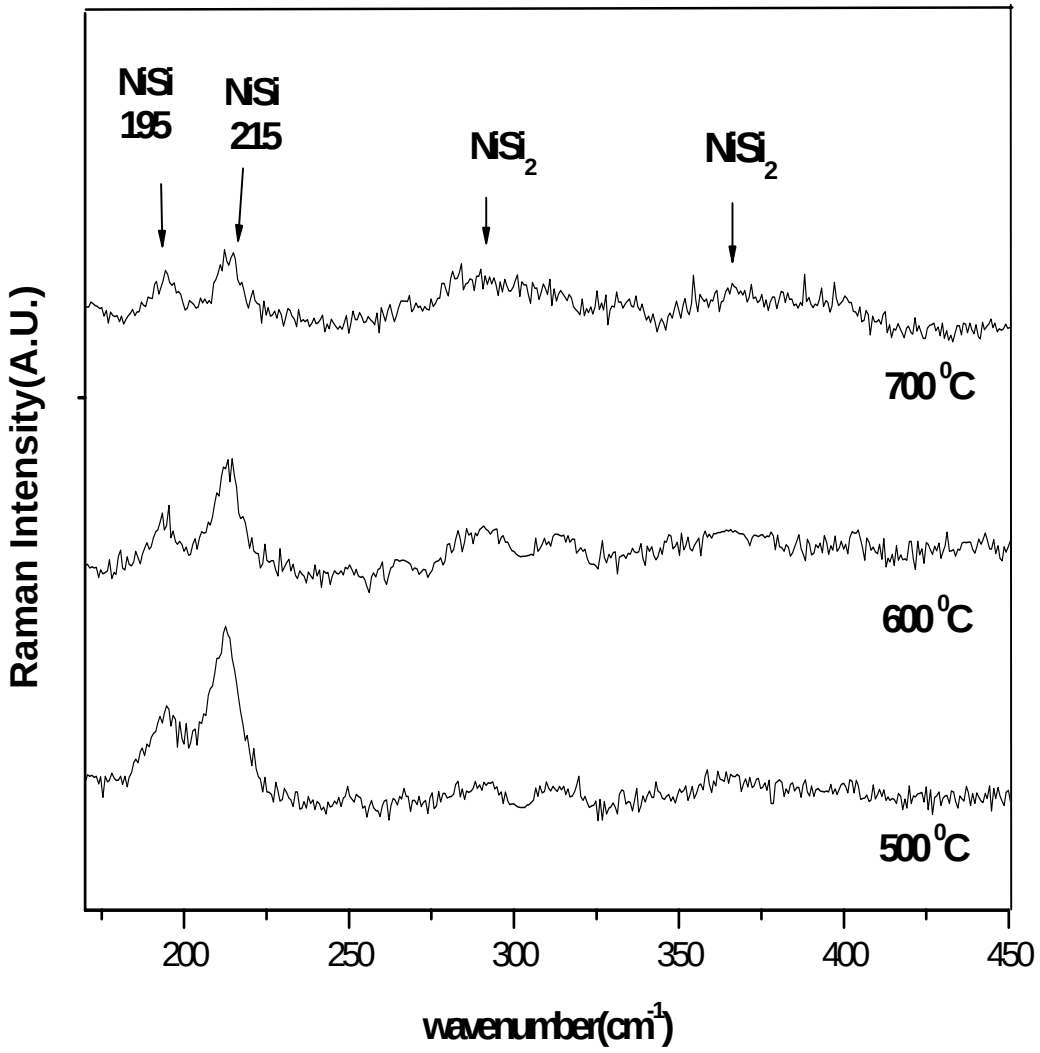

Figure 4.4 Raman spectra of Group A samples (Ni:Si=1:1) annealed at 500, 600 and 700°C for 60S.

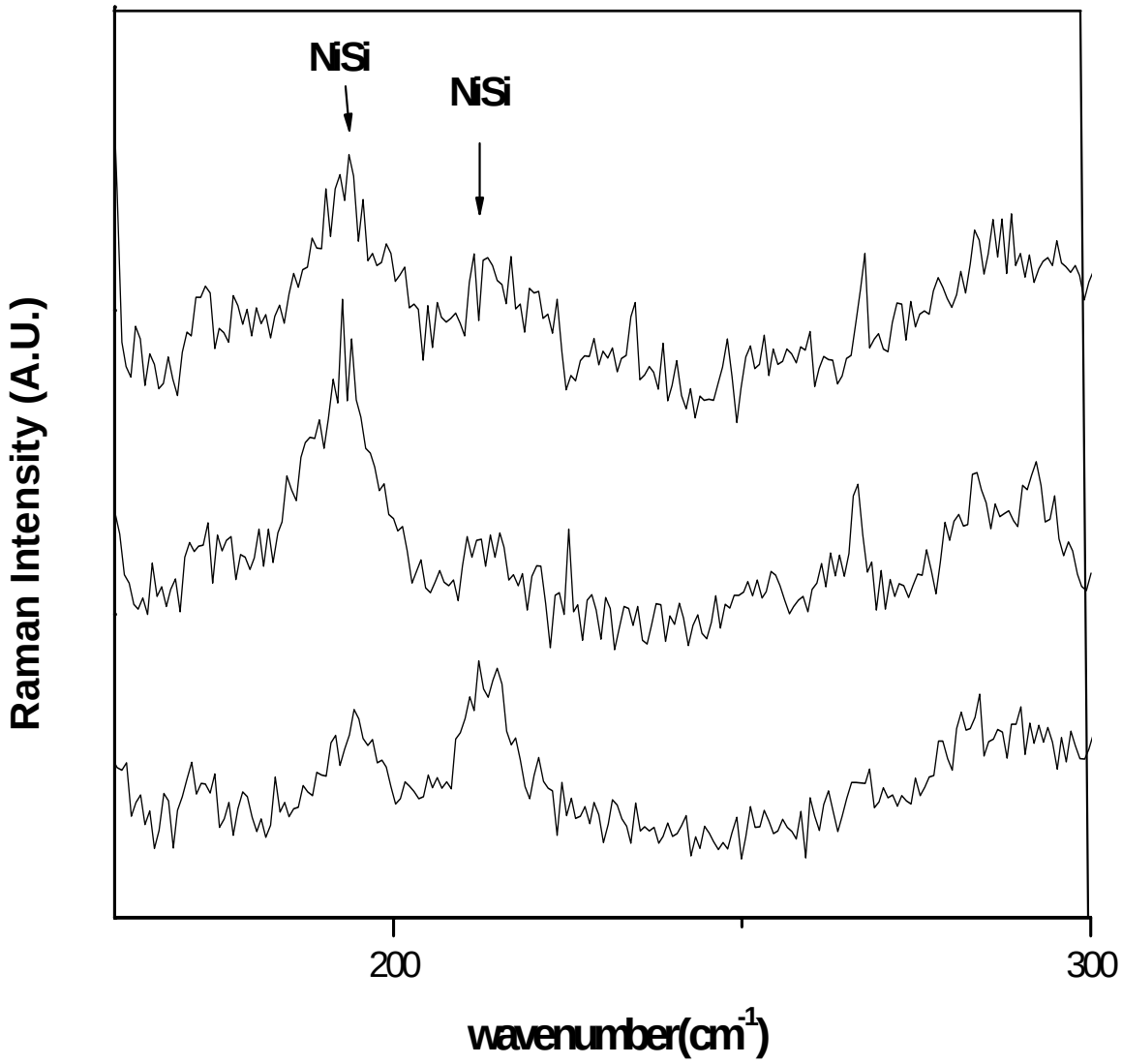

Figure 4.5 Raman spectra recorded at 3 different points from a Group A sample (Ni/Si=1:1) annealed at 700^{o}C for 60s.

NiSi belongs to the orthorhombic structure and has strong first order Raman peaks.

There has also been prior work by others on Raman study of orthorhombic silicide thin film such as $TiSi_2$ and PtSi. NiSi possesses two major peaks at 195cm^{-1} and 215cm^{-1} [4.1]. Figure 4.4 shows Raman results of the Group A samples annealed at different temperatures. The Raman spectra obtained for samples after annealing at temperatures ranging from 500 to 600°C were similar, with a strong peak at 215cm^{-1} and a lower intensity peak at 195cm^{-1} since NiSi is normally formed at 400°C and is stable below 700°C. For the samples whose Ni/Si ratio is 1:1 (Group A), the consumption of the Si substrates can theoretically be completely eliminated. When the sample was annealed at 700^{o}C, the two peaks for NiSi is weaker than those of the sample annealed at 600^{o}C, indicating $NiSi_2$ formation occurred. We recorded three Raman spectra at different points of the same sample (Fig. 4.5). In Fig 4.5 and 4.6, the Raman spectra clearly show a mixture of the NiSi and $NiSi_2$ phases. In these three spectra, it can be seen that the intensity ratio of two peaks changed obviously. In Fig 4.5, we can see that the peak at 215cm^{-1} almost disappeared, but the one at 195cm^{-1} did not decrease obviously. Similar results were observed for Group B sample (Ni:Si=2:1, Fig 4.7) and Group C sample (pure Ni, Fig 4.8). The relative Raman signals intensity is different for different thin film orientation. After annealing at 500^{o}C or 600^{o}C, stable NiSi is formed. After annealing at 700^{o}C, the dominant phase formed is not NiSi, but $NiSi_2$. The Raman spectra (Fig 4.5 and Fig 4.6) and the XRD result (Fig 4.9) show that the silicide film comprises mainly $NiSi_2$ and a small percentage of NiSi. The NiSi orientation in sample annealed at 700^{o}C is different from the one in the

sample annealed at 500°C and 600°C. So the intensity ratio of the two Raman peaks for the samples annealed at 700°C is different from those for the samples annealed 500°C and 600°C. In the next chapter, the XRD and rocking curve results prove that Group A and B samples annealed at 500°C and 600°C possess the preferred orientation of NiSi (001).

In Fig 4.8, Raman spectra of Group C samples show similar results to Group A. In the next chapter, it is proved that Group C sample annealed at 500°C or 600°C has random local orientation, so the two NiSi Raman peaks intensity ratios for samples after 500°C and 600°C annealing are slightly different from each other.

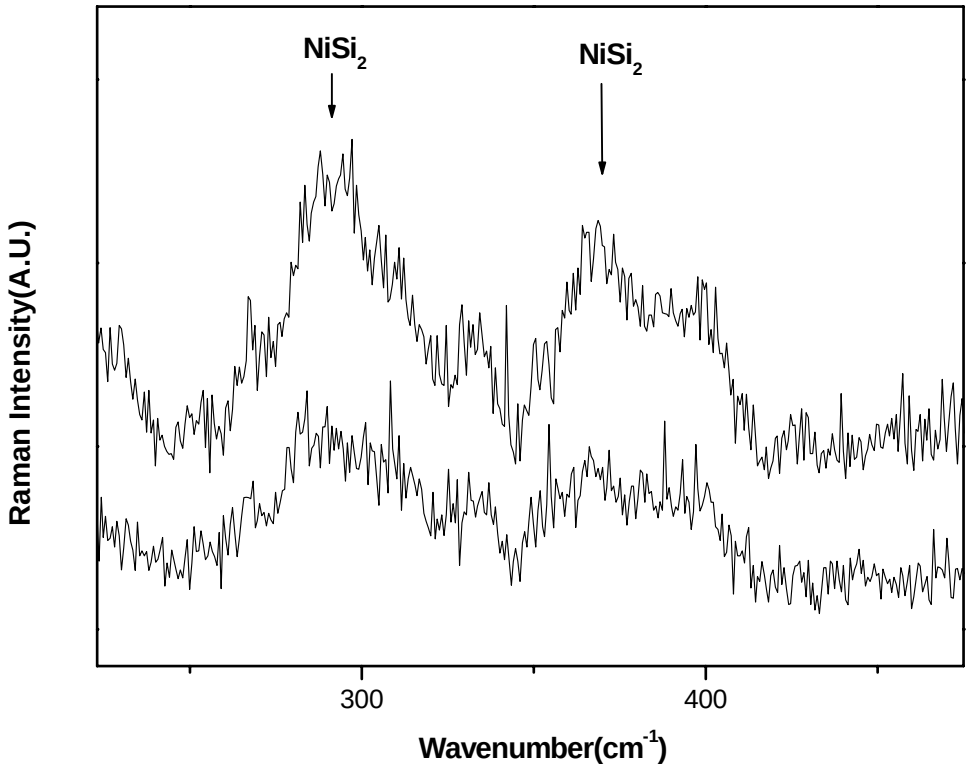

Figure 4.6 Raman spectra from two different points of a Group A Sample annealed at 700^{o}C for 60s.

$NiSi_2$ (space group Fm3m, O_h^5) has a cubic structure (CaF_2 type), which is the same as that of $CoSi_2$. It gives weak and broad second order Raman peak ranging from 250-400 cm^{-1} in Figure 4.5 [4.1].

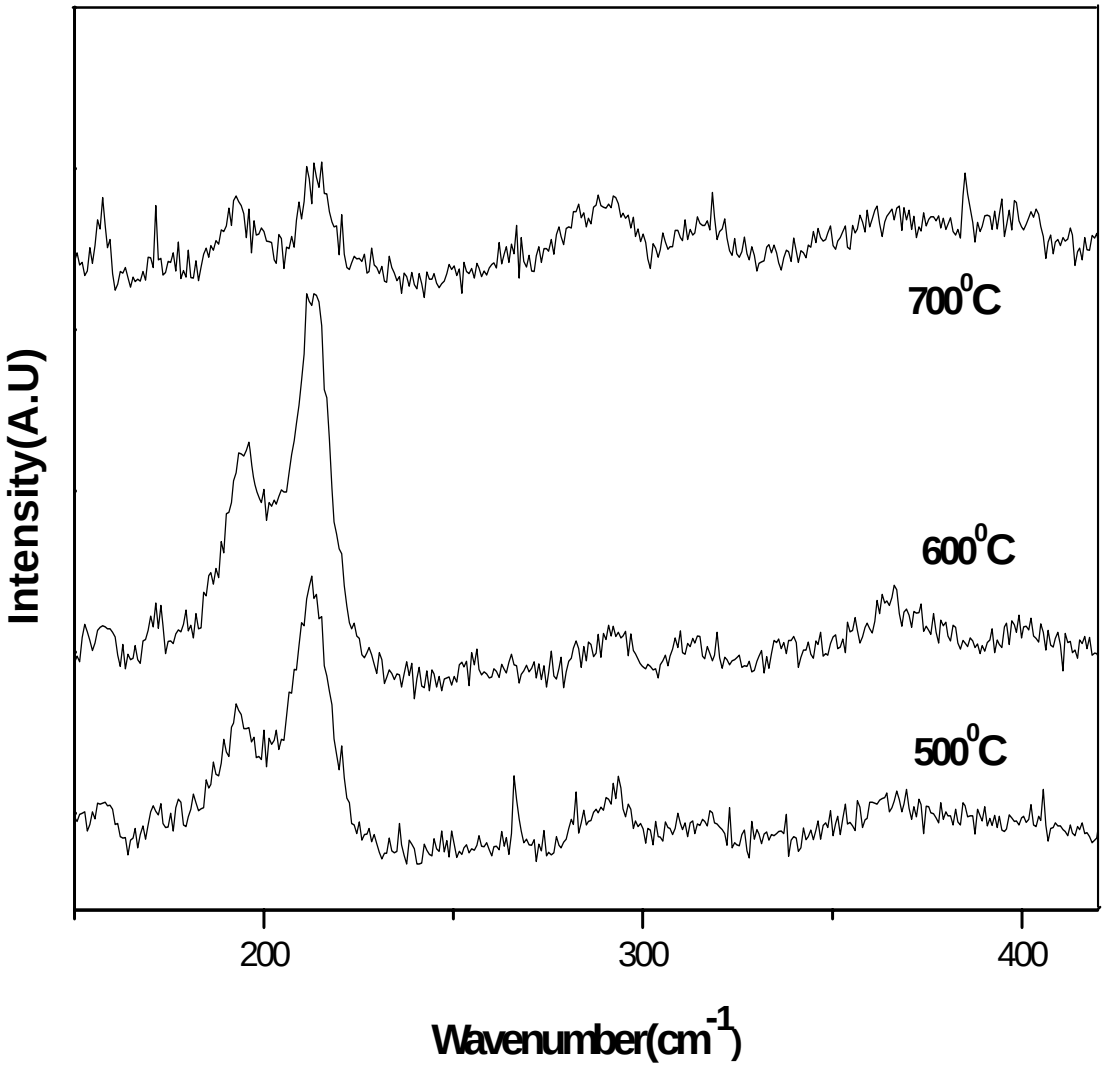

Figure 4.7 Raman spectra of Group B samples (Ni:Si=2:1) annealed at 500,

600 and 700^{o}C for 60s.

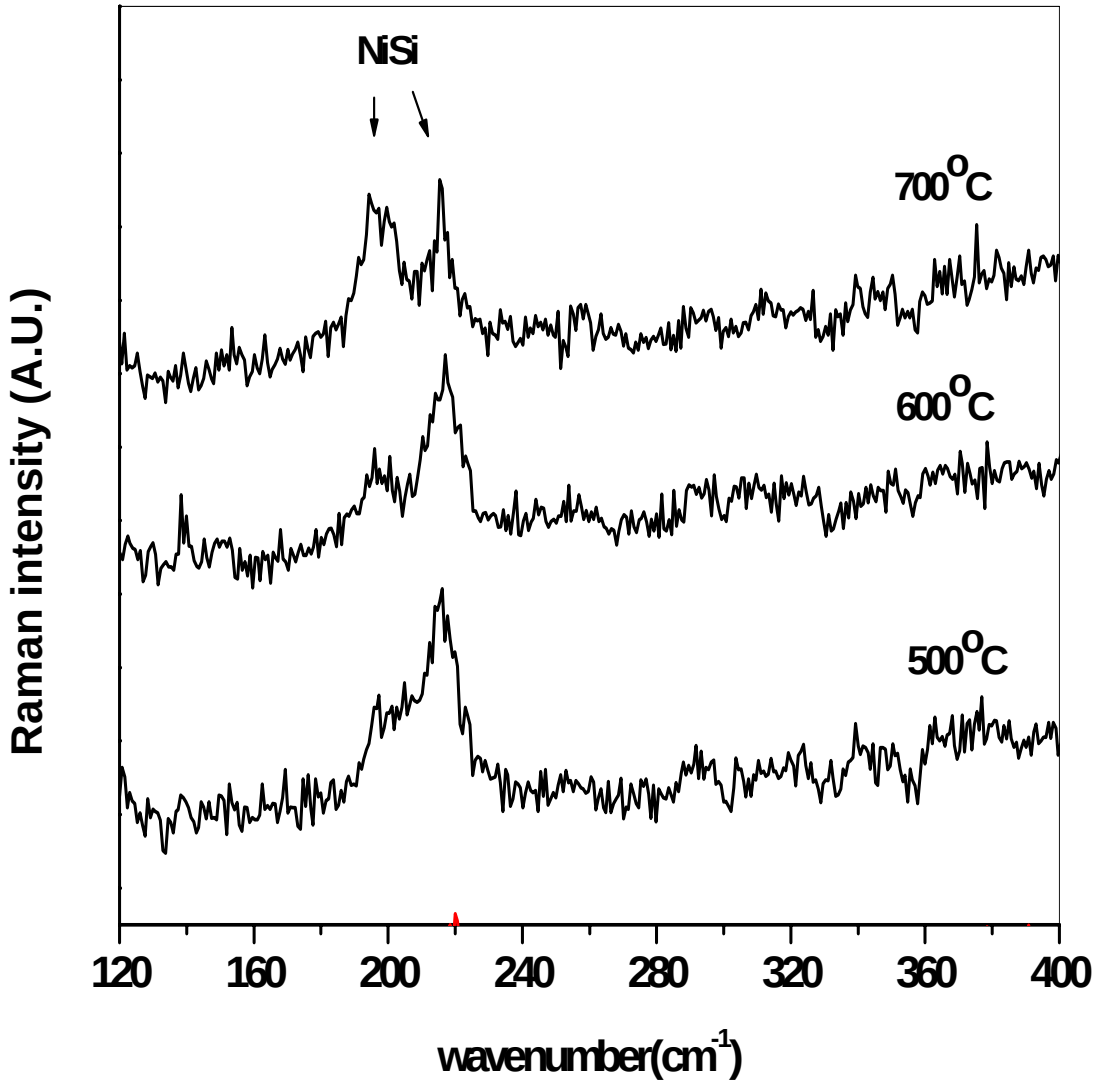

Figure 4.8 Raman spectra of Group C samples (Pure Ni) annealed at 500, 600 and 700^{o}C for 60s.

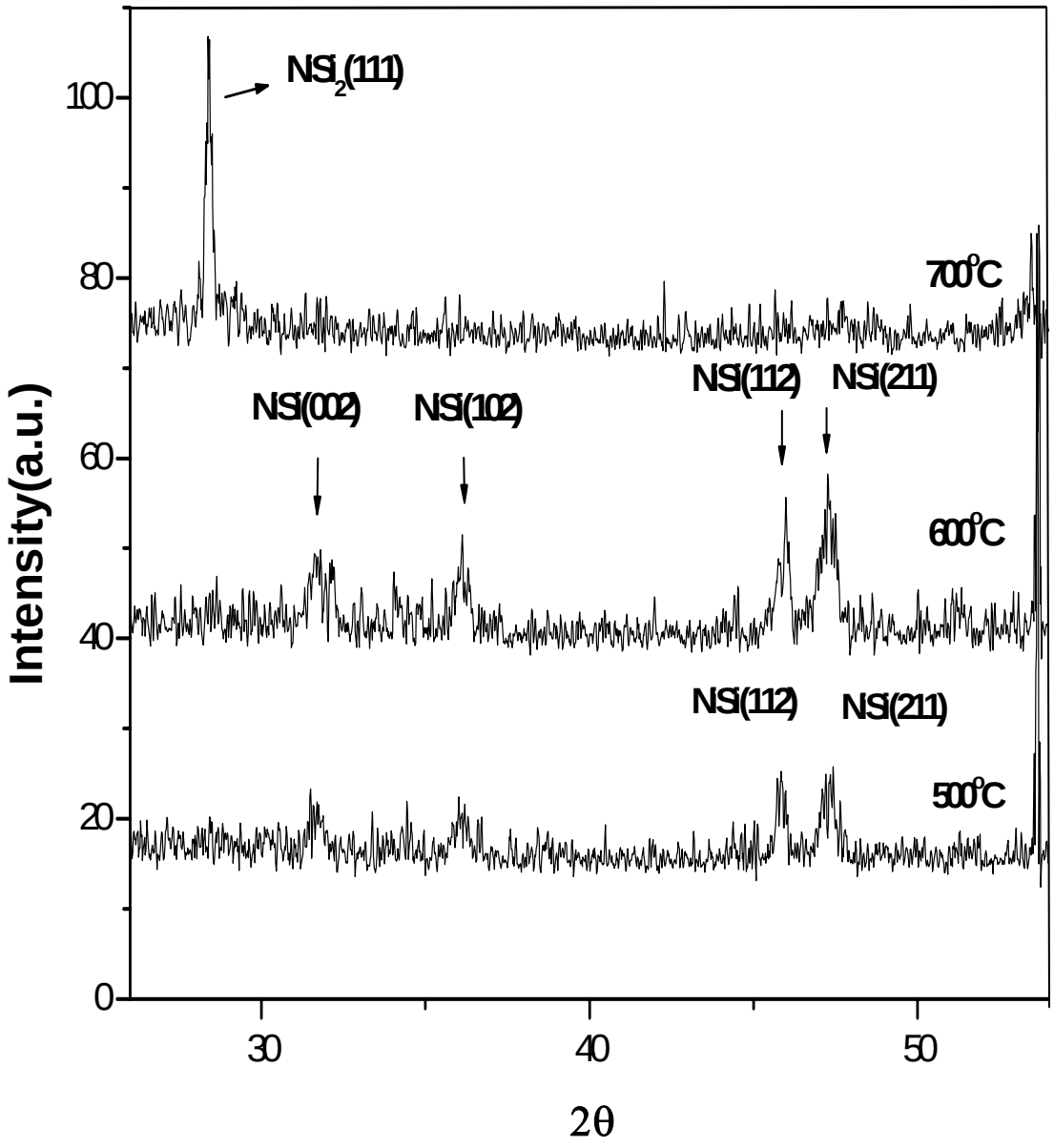

Figure 4.9 GAXRD patterns of Group B annealed at 500, 600 and 700°C for 60s

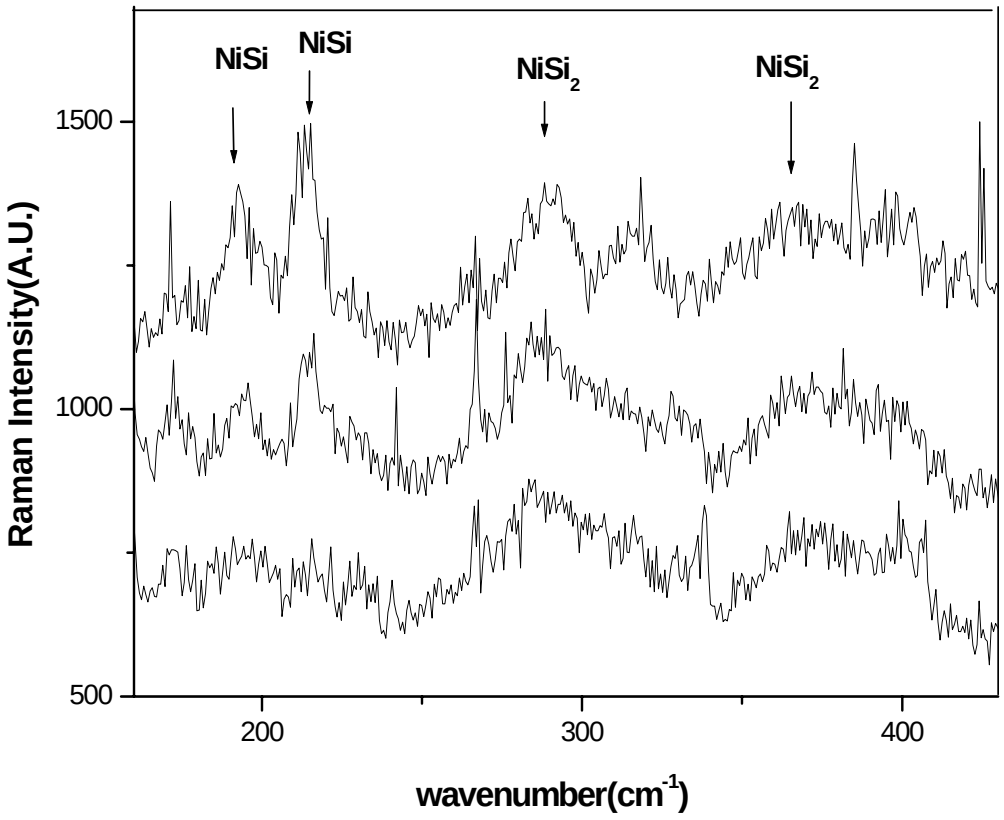

Figure 4.10 Raman spectra recorded from 3 different points of a Group B (Ni:Si=2:1) sample annealed at 700°C for 60s.

In XRD result（Fig 4.9）for Group B sample annealed at 700°C, the peak of $NiSi_2$ is very obvious, but there is no peak corresponding to NiSi. The Raman spectra (Fig 4.10) shows that the Group B sample (annealed at 700°C) shows mixture phases of NiSi and $NiSi_2$. Weak and broad peak ranging from 250-400 cm^{-1} is the signal of $NiSi_2$, while the NiSi is very easy to identify using Raman, to Raman $NiSi_2$ is not sensitive phase. XRD and Raman are complementary to each

other in Ni silicide phase identification and each of them is particularly sensitive to one of the two phases.

4.4 NiSi thin film characterization using AFM and Raman imaging

For Group A and C samples, AFM and Raman mapping were carried out. A accurate information about the surface and thickness uniformity can be obtained using AFM and Raman mapping.

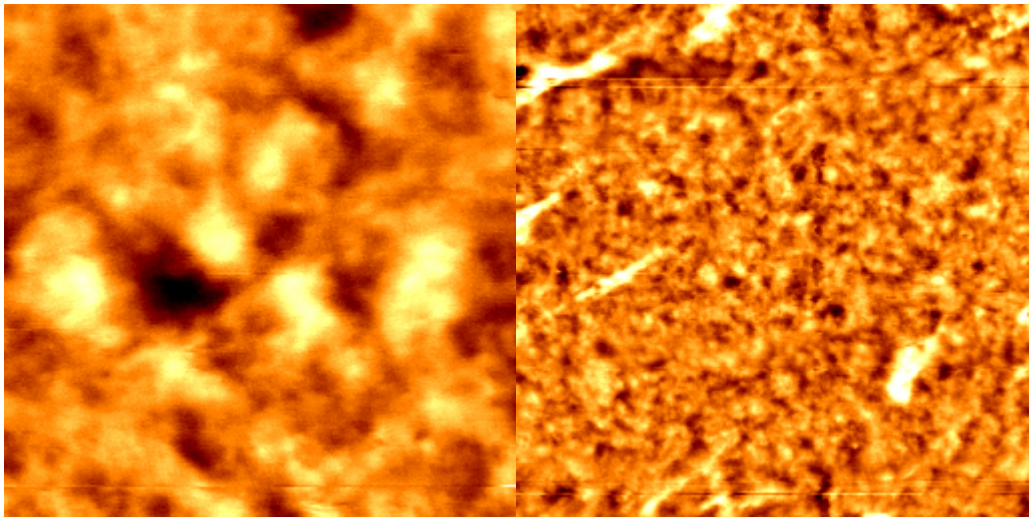

A **B**

Figure 4.11 AFM topographic images of a Group C sample annealed at 500^{o}C (A: 1µm x 1µm, RMS value: 1.1nm, Ra: 0.9nm, B: 5µm x 5µm, RMS value: 1.5nm, Ra: 1.1nm)

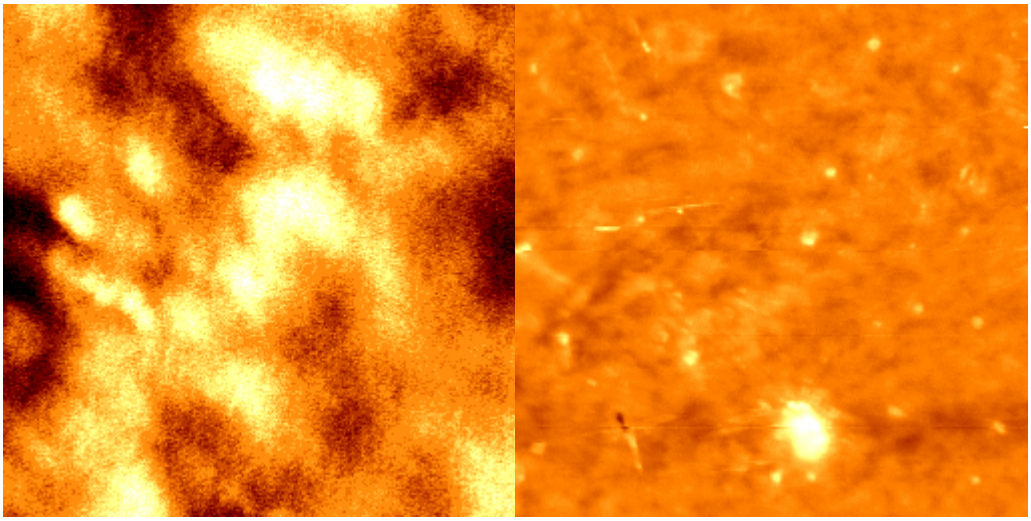

A **B**

Figure 4.12 AFM topographic images of a Group A sample annealed at 500°C (A: 1μm x 1μm, RMS value: 0.4nm, Ra: 0.3nm B: 5μm x 5μm, RMS value: 0.8nm, Ra: 0.4nm),

Arithmetic roughness Ra and RMS roughness are two parameters used to evaluate surface roughness.

$$Ra = \frac{1}{n}\sum_{i=1}^{n}\left|Z_i - \overline{Z}\right| \tag{4.1}$$

$$RMS = \sqrt{\frac{1}{n}\sum_{i=1}^{n}\left|Z_i - \overline{Z}\right|^2} \tag{4.2}$$

The most frequently used parameter is RMS. The advantage of RMS is not only its simplicity, but also the statistical significance. RMS describes the spread of height distribution about the mean value. In Fig 4.11 B (5μm x 5μm), the RMS roughness of the Group C annealed at 500°C is 1.5nm, and Ra is 1.1nm. While in Fig 4.11 B

(5μm x 5μm), the RMS roughness of Group A sample annealed at 500 ^{o} C is 0.8nm, and Ra is 0.4nm. It is apparent that Group A samples are smoother than Group C samples. In both Fig 4.11 and Fig 4.12, Fig A is extracted from Fig B area. In Fig 4.12 A (1μm x 1μm), The RMS value is 0.4nm and Ra value is 0.3nm. In Fig 4.11 A (1μm x 1μm), The RMS value is 1.1nm and Ra value is 0.9nm.The RMS value shown in Fig 4.11 A and Fig 4.12 A further confirmed that Group A samples are much smoother than Group C samples in surface. Normally, the RMS value of NiSi thin film grown by other methods is similar to Group C sample. In F. F. Zhao's work, RMS value of NiSi thin film prepared by sputtering is 1.3nm [4.2]. So the Group A sample is very smooth in surface since its RMS value (1μm x 1μm) is only 0.4nm.

Micro-Raman imaging can be used to characterize the thin film interface roughness without any special sample preparation. In this section, we performed Raman mapping to evaluate the thickness uniformity of Group A samples. When a laser beam penetrates a layer of metal or silicide thin film, it is exponentially attenuated by the film due to absorption. The laser intensity should follow this formula:

$$I/I_o = \exp(-ad) \qquad (4.3)$$

Where a is Extinction Coefficient, and d is thin film thickness. The Extinction Coefficient of NiSi is 0.1174 nm^{-1} [4.2]. Subsequently the scattered Raman signal of the Si substrate is exponentially attenuated again by the same layer before

collection by the objective in the backscattering configuration. The thin film thickness uniformity can be evaluated using the relative intensities of the Raman signals of Si substrate.

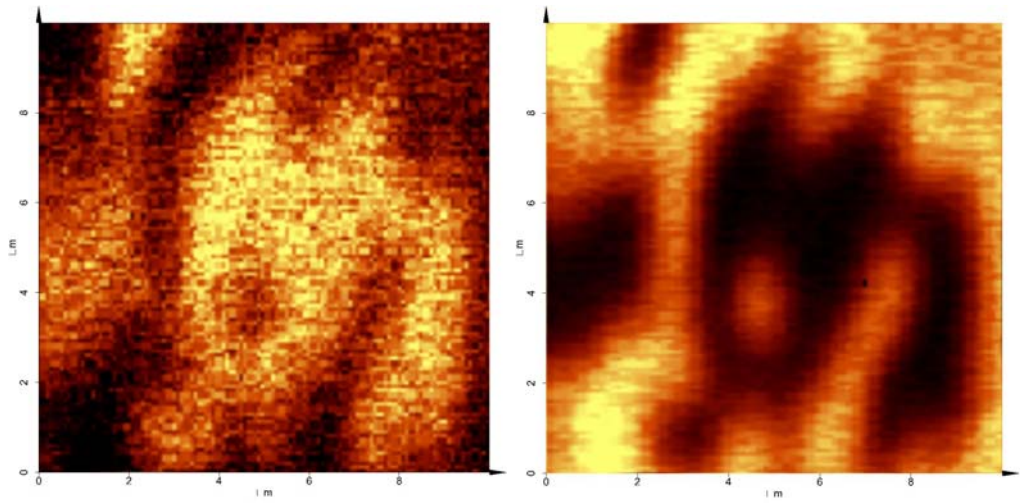

A B

Figure 4.13 Micro-Raman images (10μm x 10μm) of a Group A sample (Ni:Si=1:1) annealed at 600 °C for 60 s. A: The intensity of the NiSi Raman peak at 215 cm^{-1} (signal range: 245-391 counts) B: the intensity of the Si substrate Raman peak at 520 cm^{-1}. (Signal range: 764-1820 counts)

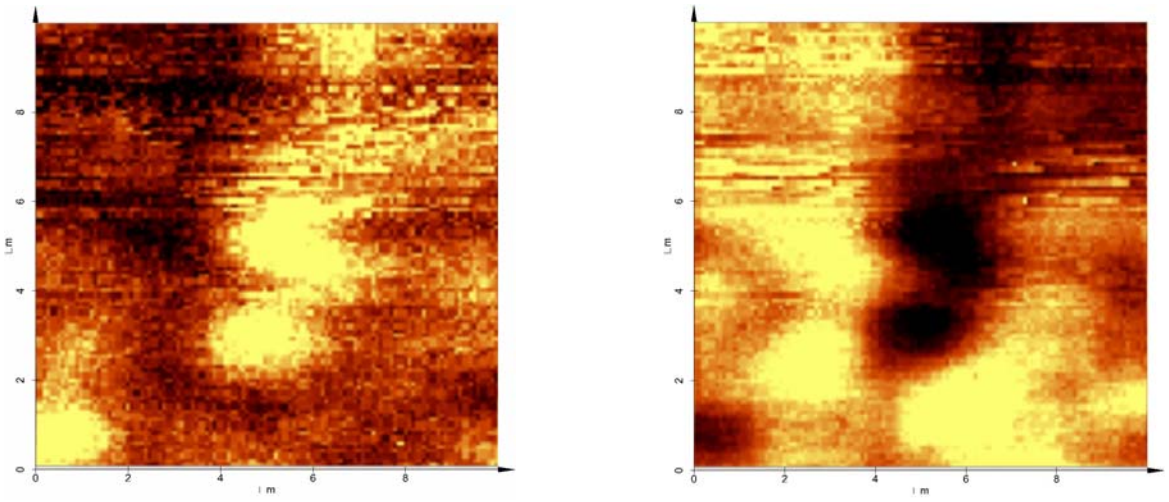

A B

Fig. 4.14 Micro-Raman images (10μm x 10μm) of the same Group A sample as in Fig 4.10, but imaged in another area. The intensity of the NiSi Raman peak at 215 cm^{-1} (signal range: 249-387 counts). B: the intensity of the Si substrate Raman peak at 520 cm^{-1}. (Signal range: 692-1481 counts)

Figure 4.13 and 4.14 showed the micro-Raman images of a Group A sample (annealed at 600 °C for 60 s) for two different areas. Fig 4.13 B and Fig 4.14 B are the images mapping the intensities of the Si 520 cm^{-1} peak for the two areas. The intensity is a reflection of film thickness of the measured area. Here brighter regions of the image correspond to thinner film, and darker parts correspond to thicker film. Based on Eqn. 4.3, I and $I_{o,}$ are known, the thin film thickness can be calculated. Since our purpose is to evaluate the thickness uniformity, the absolute thickness was not calculated. Using the Si Raman signal range, the silicide film thickness difference between the thinnest point and thickest point (named as T)

can be deduced using eqn. 4.3. Take Fig 4.13 as example, Si signal range is 764-1820 counts.

$I_1/I_o = \mathrm{Exp}(-a d_1)$ (4.4)

$I_2/I_o = \mathrm{Exp}(-a d_2)$ (4.5)

$T = d_1 - d_2$ (4.6)

Where I_1=764, I_2=1820, and a=0.1174 nm^{-1}. Eliminating I_o, T could be calculated.

T=7.8nm. (4.7)

Si substrate Raman signal yields the information of thickness uniformity which is a combination of surface roughness and NiSi/Si interface roughness. If the surface is much smoother than the interface, the thickness uniformity is an effective reflection of NiSi/Si interface roughness. In AFM results, we know that although Group A sample possesses of low RMS value; it occasionally has some points whose height is comparable to 7.8nm. So the interface roughness may not be reflected very effectively.

The Group A samples were formed with very little Si consumption from substrate during annealing. Theoretically, if the Ni/Si ratio is exactly 1:1, a single-crystalline interface with the Si substrate can be obtained. Hence, the interface of Group A sample should be relatively smooth.

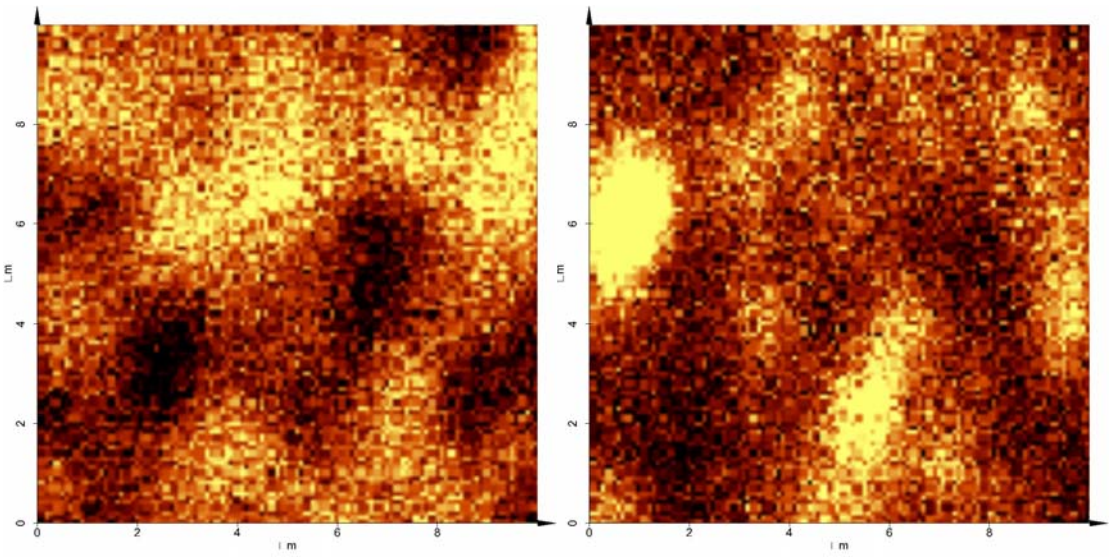

A **B**

Fig. 4.15 micro-Raman images (10μm x10μm) of the same Group C sample (pure Ni) annealed at 600°C. A: The intensity of the NiSi Raman peak at 215 cm^{-1} (signal range: 345-465counts). B: the intensity of the Si substrate Raman peak at 520 cm^{-1}. (Signal range: 117-307 counts)

In addition to Si Raman signals, intensities of the major peak of NiSi at 215 cm^{-1} are derived from the same spectra. In Fig. 4.13 and Fig. 4.14 (different points of Group A), it is clear that the NiSi image and Si image correlate with each other. Where the NiSi signal is weaker, the Si signal is stronger, and vice versa.

In Fig 4.15 (Group C sample, pure Ni), The NiSi image and Si substrate image do not correlate with each other as well as Fig. 4.13 and Fig. 4.14 (Group A, Ni:Si=1:1). It is known that orientation has strong influence on the generation of Raman signals, but a relatively small effect on refractive index and absorption coefficient [4.2]. When measuring film thickness, the local grain orientation of the

silicide films should not affect the signals collected from Raman scattering of the Si substrate which varied with NiSi thickness. So the effect of local grain orientations on thickness calculation can be neglected, it may affect the intensity of NiSi Raman signals significantly. So the reason why Fig 4.15 A and B could not correlate well is the random orientation of Group C sample which is proved in the next chapter.

However, in Fig. 4.13 and Fig. 4.14, A and B correlated with each other very well. This is because Group A samples possessed preferred orientation. In the next section, we used XRD and Rocking curve results to prove that Group A samples of the preferred orientation. The correlated Raman images in Fig. 4.13 and Fig. 4.14 lend strong support to this conclusion.

Conclusion

In summary, micro-Raman spectroscopy is a very powerful, nondestructive, and convenient technique for silicides characterization in Si device fabrication. Through Raman and AFM results, we can see that NiSi thin films can be well fabricated by Pulsed Laser Deposition with different Ni/Si ratio. Using Ni and Si target together can enhance the film surface smoothness.

4.5 References

[4.1] F. F. Zhao, S. Y. Chen, and Z. X. Shen, *J. Vac. Sci. Technol. B*, **21**, 627 (2003).

[4.2] F. F. Zhao, W. X. Sun, Y. P. Feng, J. Z. Zheng, and Z. X. Shen, *J. Vac. Sci. Technol. B*, **23**, 2 (2005).

[4.3] J.A. Kittl, A. Lauwers, Chamirian, M. Van Dal, A. Akheyar, and M. De Potter, *Microelectron. Eng.*, **70**, 158 (2003).

Chapter 5

NiSi thin film characterization by X-Ray diffraction

5.1 Introduction to X-ray Diffraction theory

When a wave interacts with a single particle, the particle scatters the incident beam uniformly in all directions. What happens when a wave interacts with a single plane of regularly spaced atoms? Consider two scattered waves which are in phase, reinforcing each other to give a diffracted beam when they travel the same distance. This happens for scattered waves with an outgoing angle of: $\theta_{out} = \theta_{in}$. So a diffracted beam from a single row of atoms is made up of all the waves which are scattered with an outgoing angle equal to the incoming angle of the incident waves.

What happens if the beam is incident on solid material (Many layers of atoms)? Consider two waves C and D interacting with many layers of regularly spaced atoms. The adjacent planes are separated by a distance *d*. The diffracted beam from a single layer of atoms has $\theta_{out} = \theta_{in}$. They are in phase only if the path difference between waves C and D (in Fig 5.1, GE+EH=x+y) is an integer multiple of the wavelength. The equation for this path difference gives Bragg's law: $x + y = 2d\sin\theta = n\lambda$ This condition, which gives rise to diffracted beams, depends on the wavelength, the spacing of the planes of atoms, *d;* and the angle of incidence of the beam. This is known as Bragg's law::

$N\lambda = 2d\sin\theta$

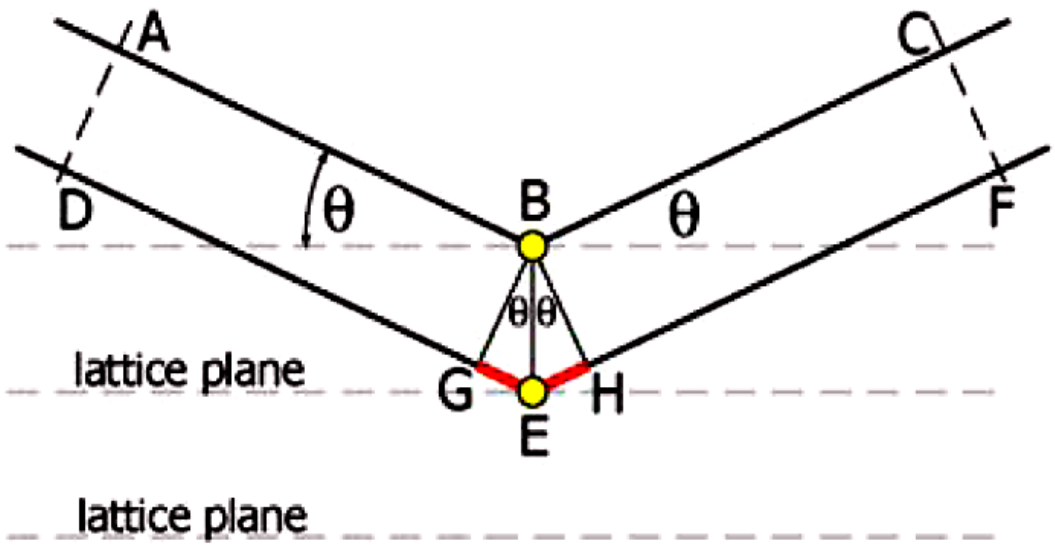

Figure 5.1 Principal of Bragg's Law.

Diffraction can occur whenever Bragg's law is satisfied. With monochromatic radiation, an arbitrary setting of a single crystal in an X-ray beam will not typically produce any diffracted beams. There would therefore be very little information in a single crystal diffraction pattern from using monochromatic radiation.

This problem could be solved by continuously varying θ or wavelength to satisfy Bragg's law. Practically this is done by: using a range of X-ray wavelengths, or by rotating the crystal, or by using powdered or polycrystalline samples.

5.2 X-Ray Diffraction (XRD) Instrumentation

Bragg Brentano geometry XRD

XRD is the most common method for determination of the crystalline microstructure of materials. It is usually used in combination with a database of known crystalline structures and an appropriate search match algorithm. The geometry generally used is the conventional θ-2θ (or Bragg Brentano) geometry in which the angle of the diffracted beam equals the angle of incidence with respect to the sample surface. A high intensity of the diffracted beam results from para-focusing whereby the process of diffraction refocuses the diffracted beam from any particular set of crystalline planes onto a slit in front of the detector. The θ-2θ diffraction geometry is shown schematically in Figure 5.2

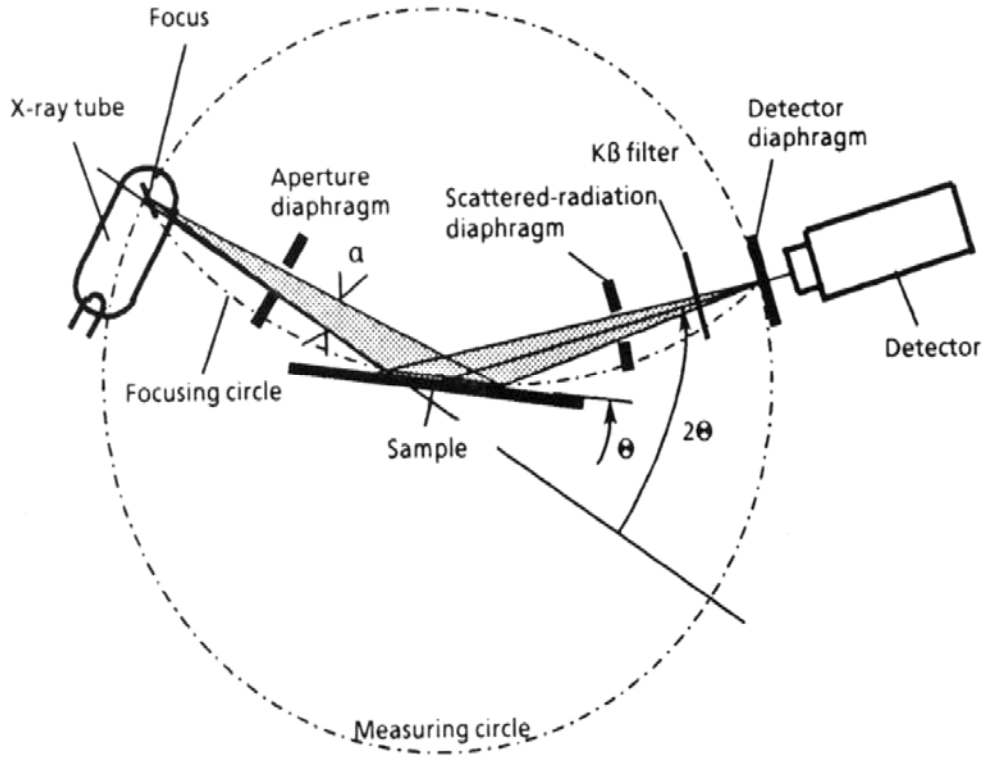

Figure 5.2 Schematic diagram of the θ-2θ Geometry X-Ray Diffraction.

Glancing angle XRD (GAXRD)

Conventional XRD systems suffer a great disadvantage when it is used in thin film analysis since the penetration depth of the X rays may be much bigger than the film thickness. The penetration depth of copper K*a* x-rays ranges from just 1μm for gold to about 500μm for graphite. When studying films which are much thinner than these values, not only is the x-ray diffraction intensity much reduced, but also scattering from the substrate may interfere with the signal from the film. For polycrystalline thin films, the solution to this problem is to use the glancing angle geometry where the

angle of incidence of the impinging beam on the sample surface is very small, and does not vary during a scan. This method destroys the conditions for Para focusing, and a Soller slit must be used in the diffracted beam to maintain a reasonable angular resolution.

This geometry is usually called the GIAB (grazing incidence asymmetric Bragg) geometry. While intensity is reduced in this way, the advantage gained in terms of increased x-ray path-length in the film and reduced substrate signal is considerable. GAXRD is about 100 times more surface sensitive than θ-2θ diffraction.

XRD is normally applied for determination of texture, stress, and crystallite size. In order to extract information from GAXRD scans concerning these parameters, it is very important to understand the fundamental difference between θ-2θ XRD and GAXRD. In θ-2θ diffraction, the diffracting planes which contribute to a diffraction peak are parallel to the surface. This makes determination of texture (preferred orientation) very simple, since the majority of thin films define the planes parallel to the surface as the preferred orientation. Hence, diffraction peaks with particularly high intensities will be from the planes of preferred orientation. On the other hand, the GAXRD geometry detects planes that are tilted with respect to the surface at an angle θ, θ being the angle of incidence; this is illustrated in Figure 5.3. This makes determination of the preferred orientation rather difficult. Furthermore, the peak representing a non-preferred set of planes will usually exhibit an abnormally high intensity.

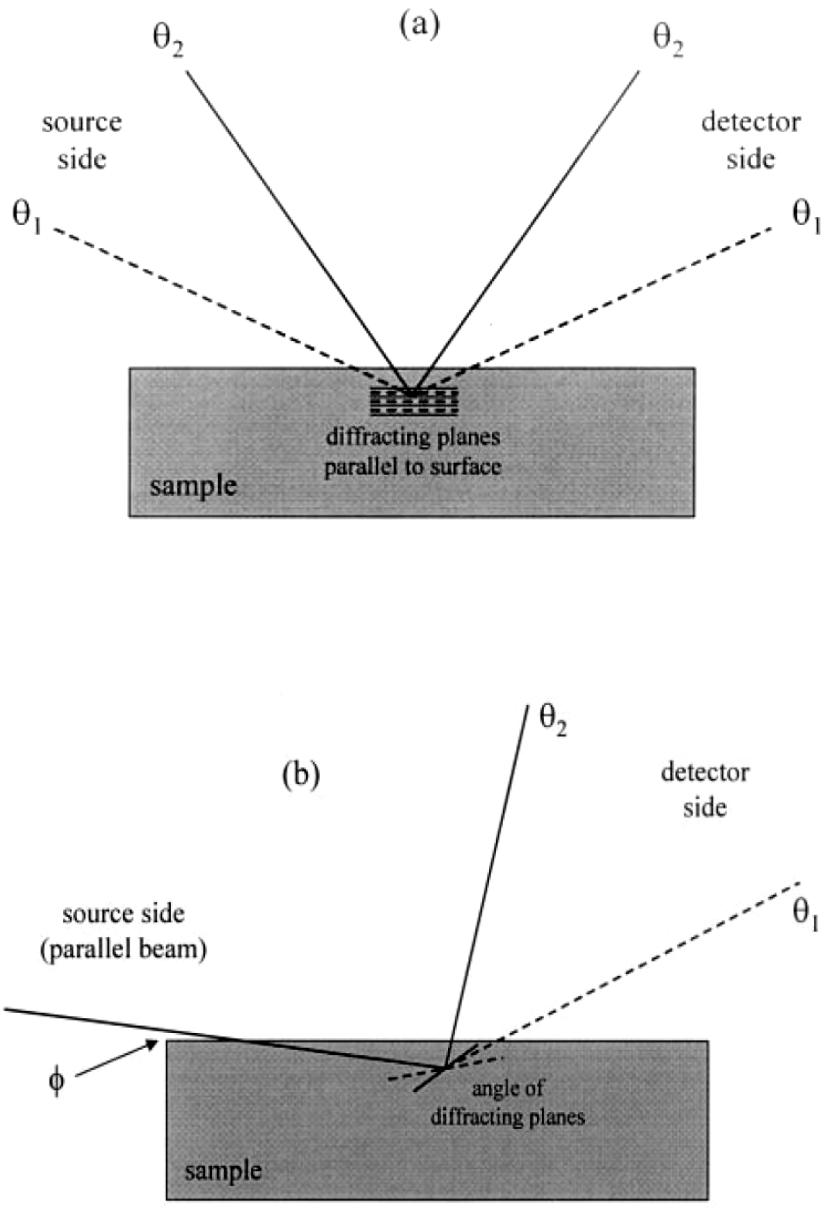

Figure 5.3 Schematic diagram of the difference between θ-2θ XRD and GAXRD (GIAB geometry) illustrating the angle of the planes detected in the measurement with respect to the sample surface.

Rocking Curve

By fixing the X-Ray source and detector in Bragg angle, $2\theta_B$, and rotating the sample through θ_B, the intensity versus θ curve can be obtained. This is known as the rocking curve. Rocking curve is an important application of XRD, which is normally used in the evaluation of thin film texture properties. The experiment setup is schematically shown in Fig 5.4. The width of the rocking curve is a direct measurement of the range of orientation present in the irradiated area of the sample.

Take a single crystal sample for example. Since the Bragg angle is fixed, Bragg scattering only happens in the preferred orientation plane (which is defined as the crystal planes parallel to the crystal surface) where the rocking curve gives a very sharp peak. A perfect single crystal sample gives a very narrow peak, of which the Full-Width-at-Half-Maximum (FWHM) is 0.05 degrees.

However, if the sample is a non-texture thin film (random local orientation), the scattering will happen in all the positions during the sample rotation. Therefore no prominent peaks will be observed in the Rocking curve. The result can also be considered as a broad "peak" with a width of 360^{o}C. This essentially means that the sample's properties in all the directions are identical.

Corresponding to above properties, rocking curve can be used in the texture thin film characterization. Texture thin film, which is also known as thin film with preferred orientation, is the crystalline structure that exhibits characteristics between that of the single crystal and non-texture film. Since texture thin film does not crystallize as perfectly as the single crystal thin film, its rocking curve peak will be wider than that

of the single crystal. Well-crystallized textured thin film gives FWHM less than 1^{o}. Thin films of the preferred orientation, but without very good crystalline quality, give FWHM values of several degrees. Therefore FWHM is an effective metric for evaluating thin film texture properties.

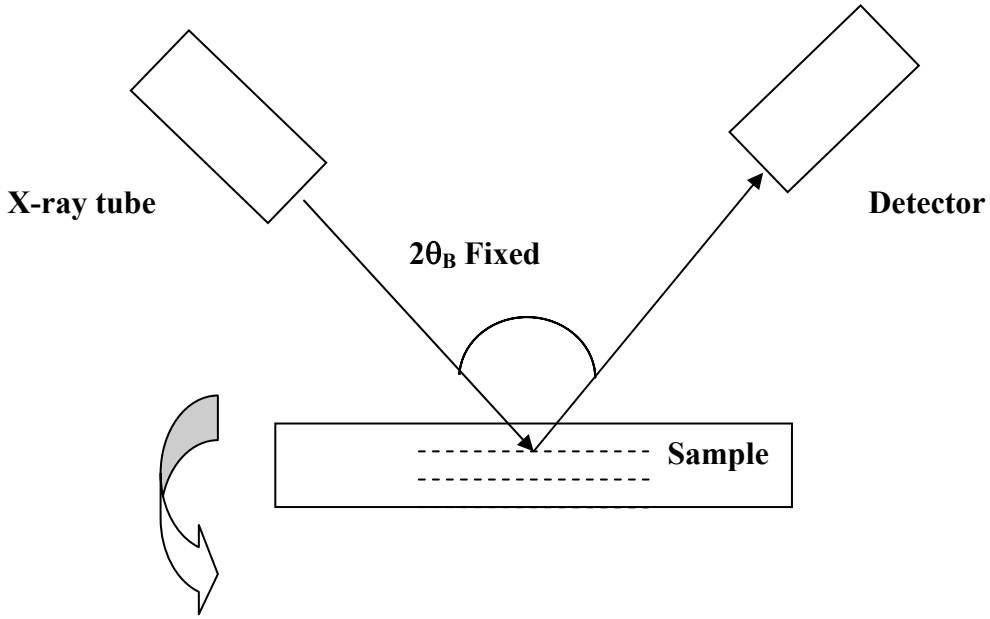

Figure 5.4 Schematic diagram of Rocking Curve experiment.

5.3 X-Ray Diffraction characterization of NiSi thin film

Figure 5.5 shows the GAXRD results of the Group A samples (Ni:Si=1:1). After annealing at 500^{o}C, NiSi was formed, as indicated by the strong NiSi (121) peak. There are also many peaks corresponding to NiSi in the spectrum for the sample annealed at 500^{o}C. On the other hand, for the sample annealed at 700^{o}C, $NiSi_2$ (111) peak is present. This is consistent with the Raman results in chapter 4.

In the last chapter, Figure 4.8 is the GAXRD result of Group B samples in which the Ni/Si ratio is about 2:1. The samples which were annealed at 500^{o}C or 600^{o}C show NiSi phase. The GAXRD result gives the peaks corresponding to NiSi (002), (102), (112) and (211). While for the sample annealed at 700^{o}C, sharp peak for $NiSi_2$ was present. These are also consistent with the Raman results in chapter 4.

In Figure 5.6, we compared the 3 groups of samples after annealing at 500^{o}C. Samples with different Ni/Si ratio are different in orientation after annealing. With the increasing of Si/Ni ratio, NiSi (211) peak becomes stronger, while the NiSi (112) peak decreases. In the XRD results of Group C, NiSi(112) peak is the strongest, whereas in Group A , the NiSi (211) peak is the strongest.

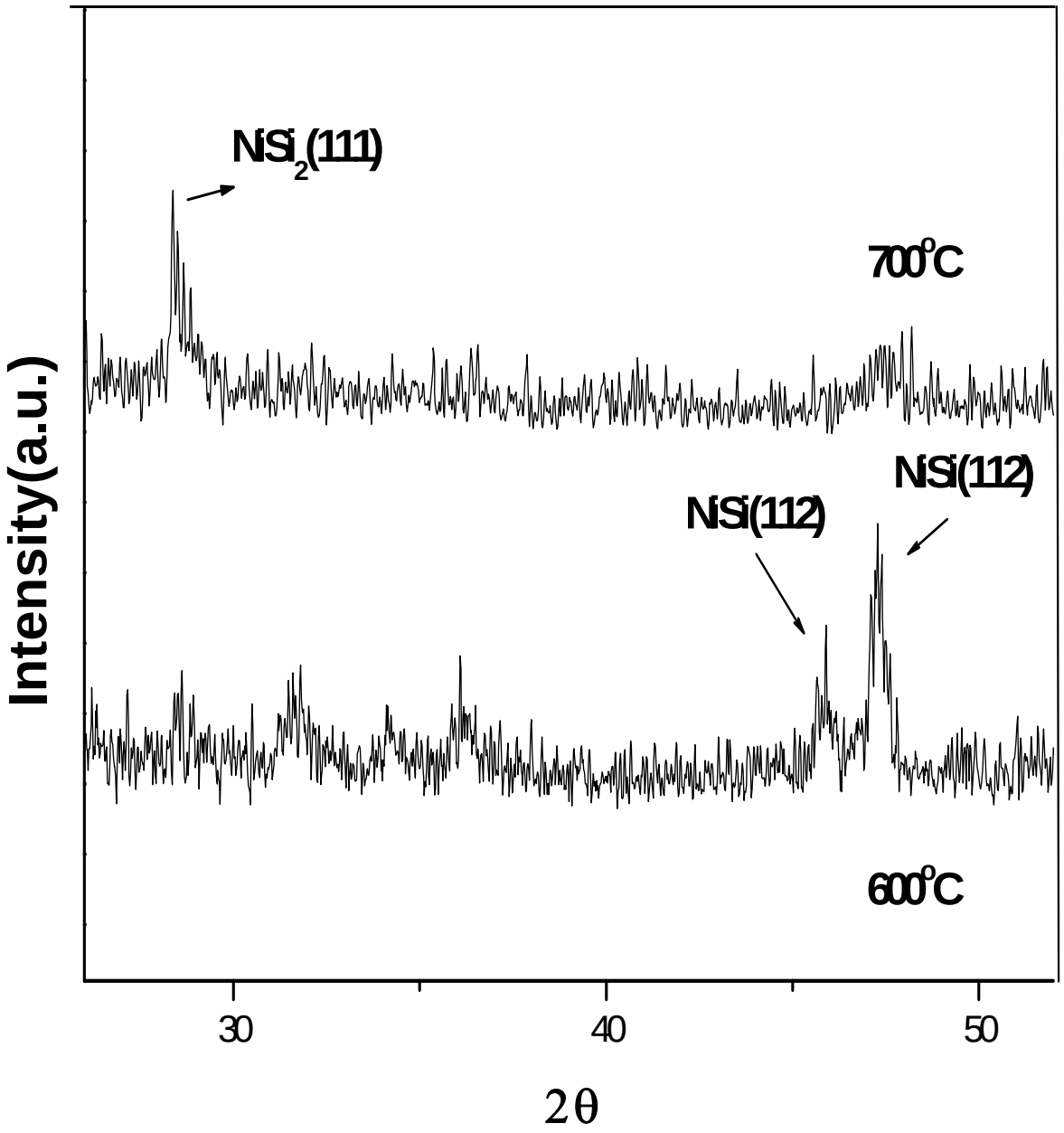

Figure 5.5, XRD patterns of Group A samples annealed at 500 and 700°C for 60s

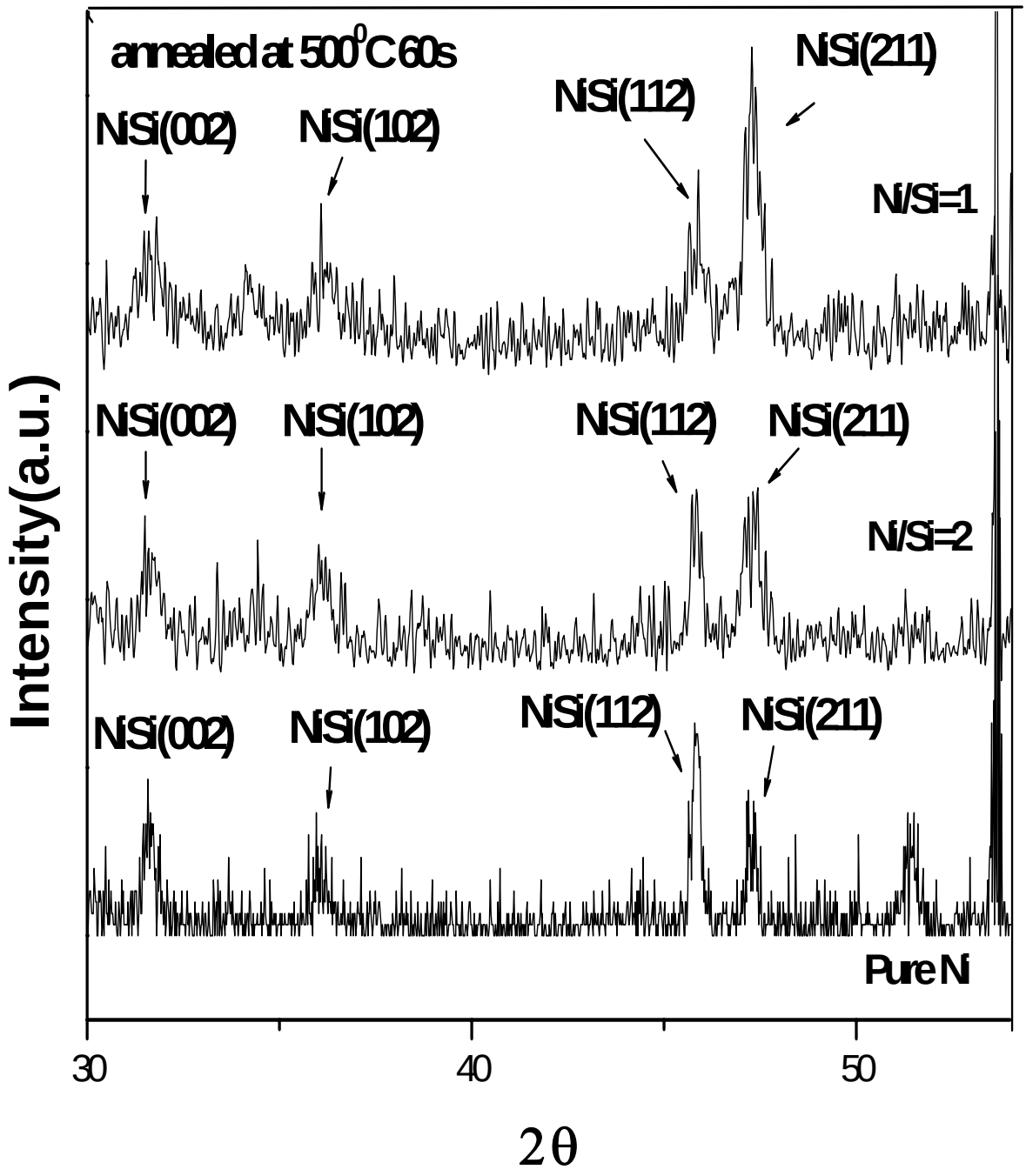

Figure 5.6 GAXRD pattern of the Group A, B, C annealed at 500°C for 60s.

Transport properties are strongly related to the micro-structure and local orientation. The GAXRD geometry detects planes that are tilted with respect to the surface at an angle of incidence. It often occurs that a peak representing a non-preferred set of planes will exhibit an abnormally high intensity [5.1, 5.2]. In theta-2 theta diffraction the angle of the diffracting planes that contribute to a diffraction peak are always parallel to the surface. This makes determination of texture (preferred orientation) extremely simple. The diffraction peak with an abnormally high intensity will be associated with planes of preferred orientation. The Bragg Brentano theta-2theta setup XRD gives the information that NiSi preferred orientation changed with the formation temperature in the Ni/Pt/Si system [5.1, 5.2].

The Ni/Si ratio effect on NiSi thin film growth orientation was also studied by Bragg Brentano (theta-2theta setup) XRD. Figure 5.7 shows the XRD results for Group A and B samples annealed at 500^{o}C. We can see a very strong peak diffracted from NiSi (002). So we conclude that the Group A and Group B were textured thin films and with a preferred orientation of NiSi (001).

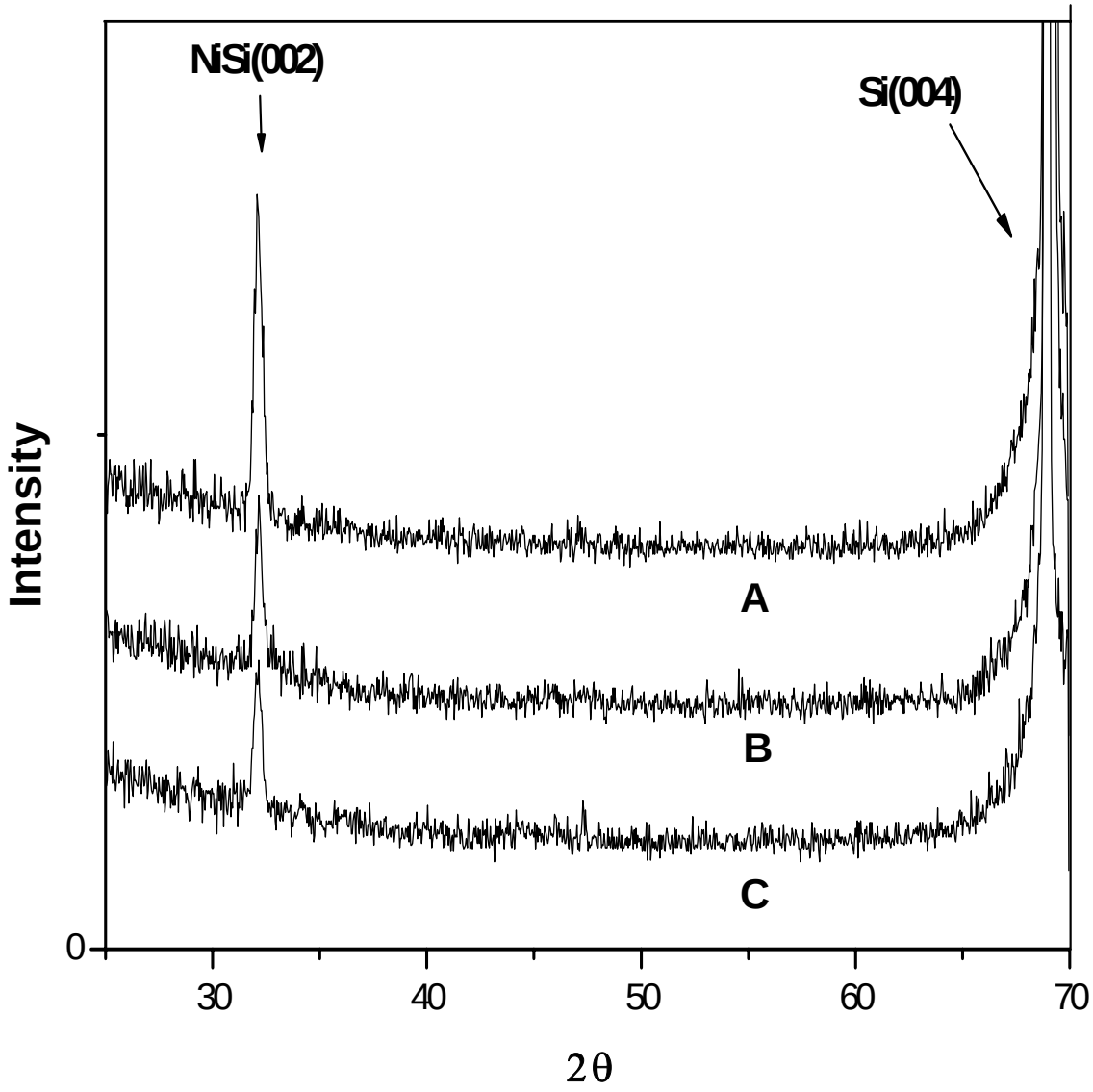

Figure 5.7 XRD patterns of Group A (Ni:Si=1:1) and B samples (Ni:Si=2:1),

A: XRD pattern of a Group A sample annealed at 500^{o}C for 60s,

B: XRD pattern of a Group A sample annealed at 600^{o}C for 60s,

C: XRD pattern of a Group B sample annealed at 500^{o}C for 60s.

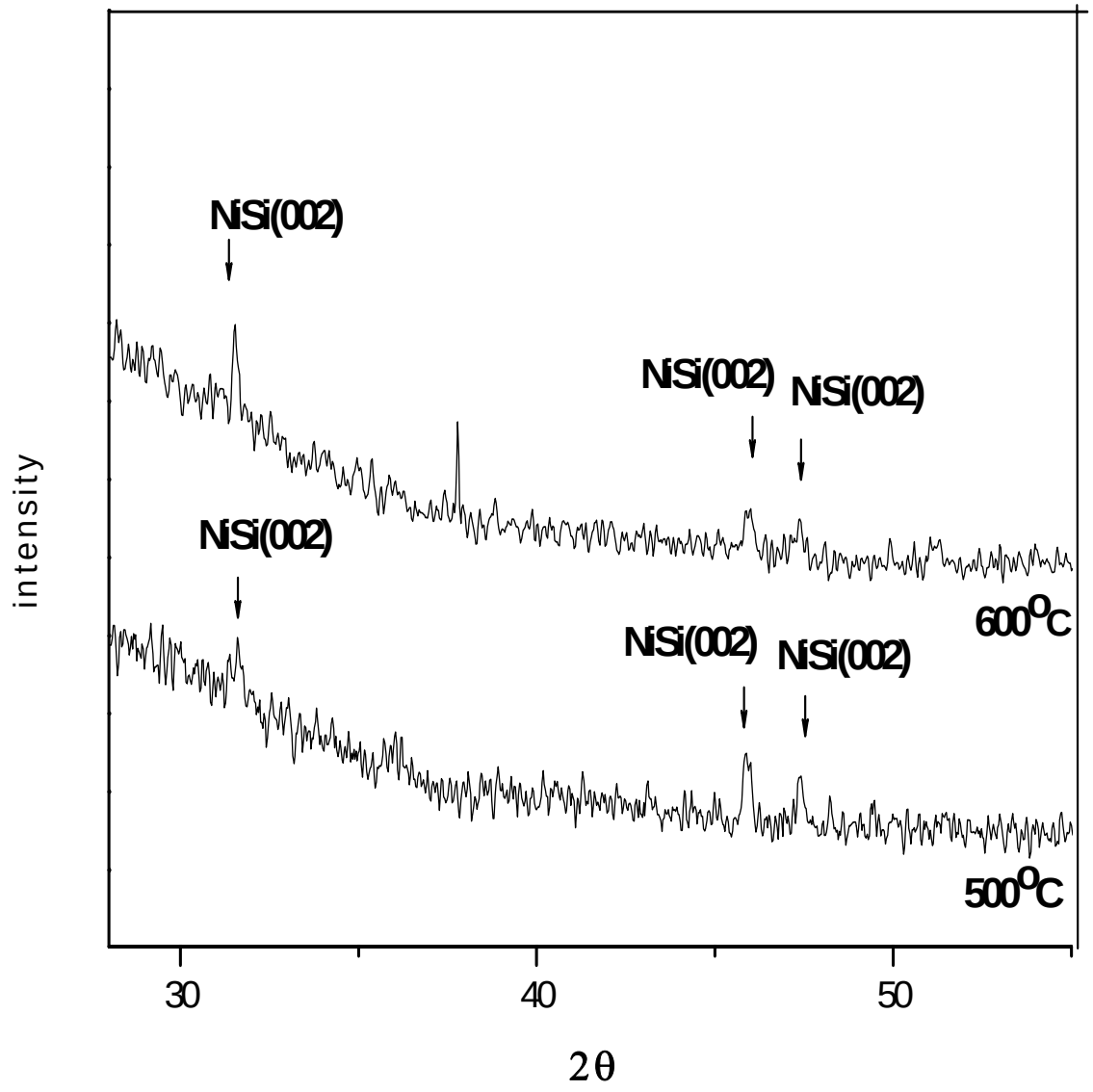

Figure 5.8 XRD patterns of Group C samples (pure Ni) annealed at 500 and 600°C for 60s.

In figure 5.7, the preferred orientation NiSi (002) of the thin film can be seen easily. For the Group A samples, the one annealed at 600°C shows a stronger NiSi (200)

peak than the one annealed at 500^{o}C. The main reason is that the thin film crystallized better and possessed better texture properties at higher annealing temperature.

In figure 5.8, we can see peaks corresponding to different orientation of NiSi. This further proves that Group C samples possess relative random orientation. These results agree with previous work done by others [5.2, 5.3].

For Group C samples, Ni should diffuse into single crystal Si wafer and react with Si to form NiSi during annealing [5.5]. For Groups A and B, Ni reacted with the as-deposited amorphous Si in the thin film during annealing first. The orientation difference is due to the different reaction mechanisms. The NiSi thin films fabricated by our method possess the preferred orientation.

The Rocking Curve was done to evaluate the texture properties. The effect of annealing temperature and Ni/Si ratio on texture properties can also be studied by this method. The rocking curves were mainly done on the preferred orientation of NiSi (002).

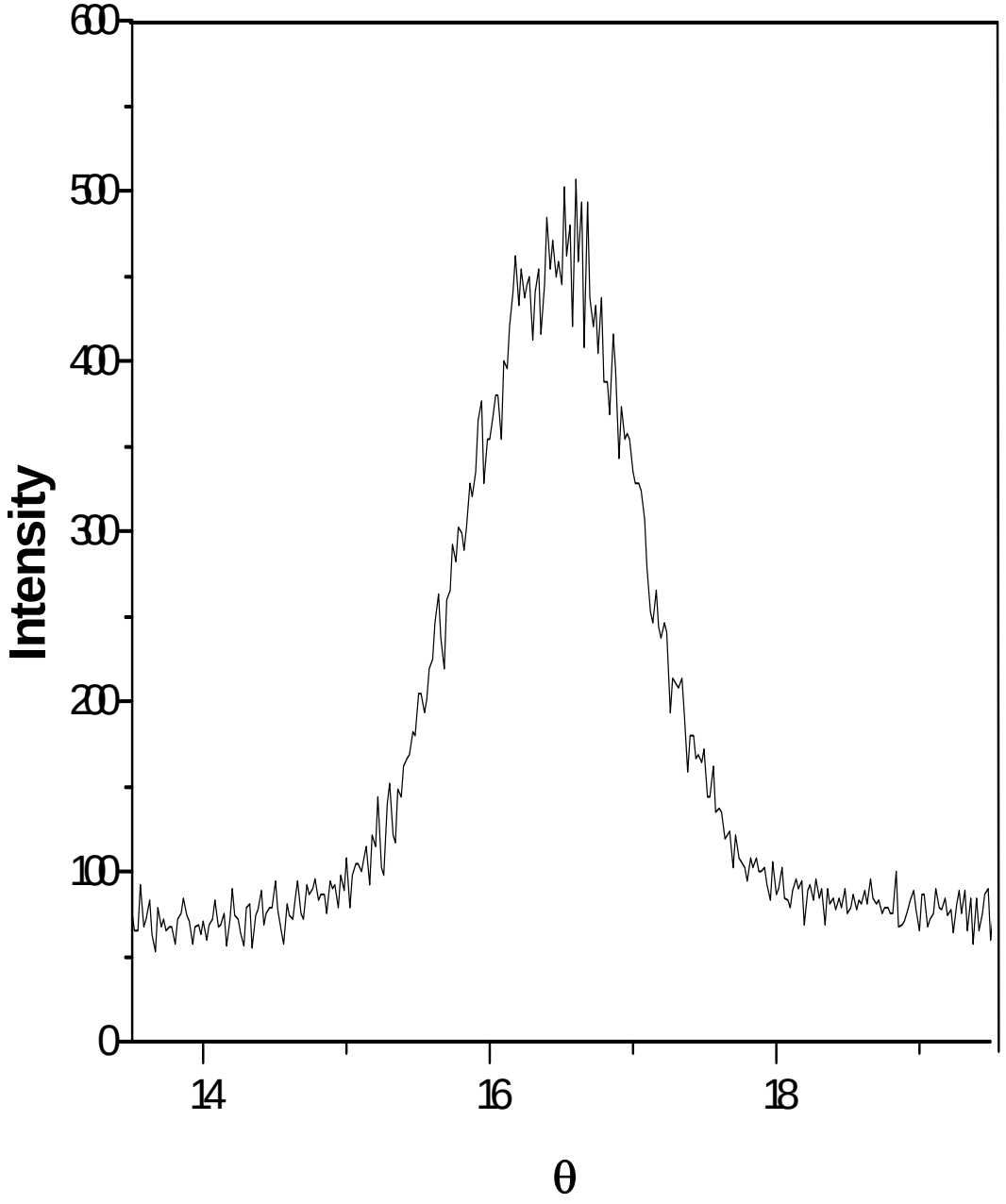

Figure 5.9 Rocking curve of a Group A (Ni:Si=1:1) sample annealed at 600^{o}C for 60s

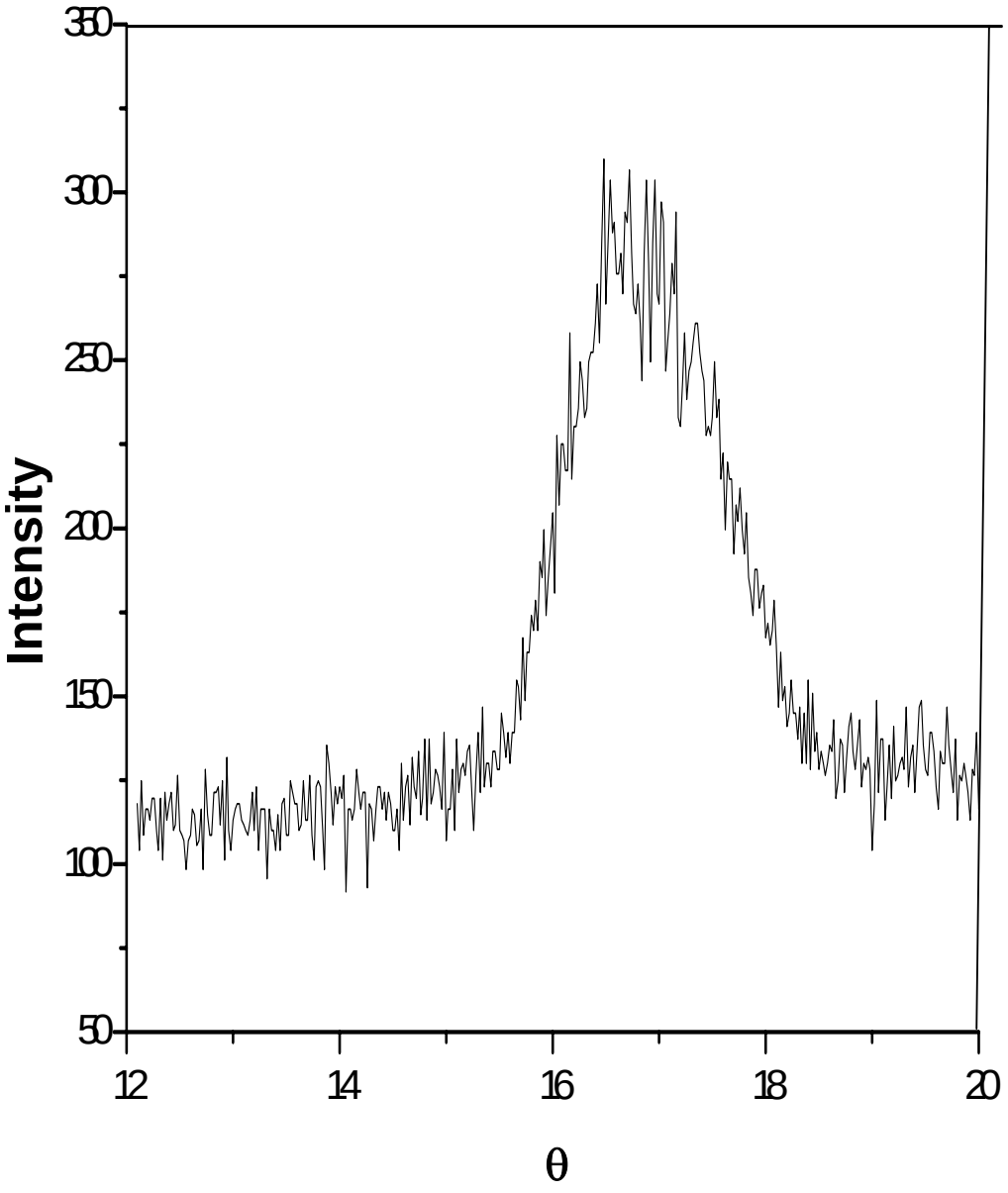

Figure 5.10 Rocking curve of a Group A sample (Ni:Si=1:1) annealed at 500°C for 60s.

In Figure 5.9，Rocking curve results confirm that the NiSi thin film is of a preferred orientation. The FWHM of peak is 1.30^{o}. It was found that the FWHM value is a function of annealing temperature. As shown in Figure 5.10, a larger FWHM value 1.67 ^{o} was obtained for the thin films annealed at lower temperatures. The FWHM difference between the films annealed at 500 and 600^{o}C proved that the thin film crystallized better when annealed at higher temperature.

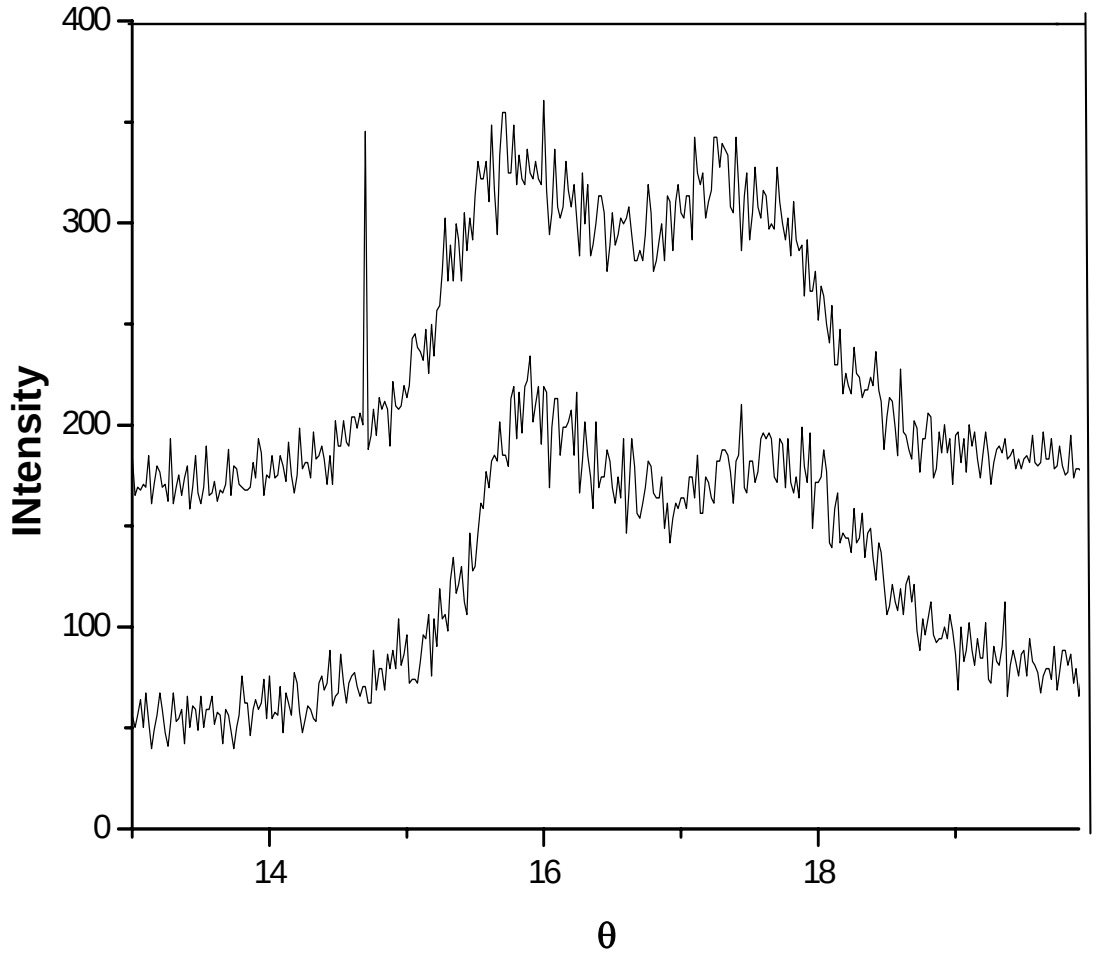

Figure 5.11 Rocking curve of a Group B sample (Ni:Si = 2:1) annealed at 500^{o}C

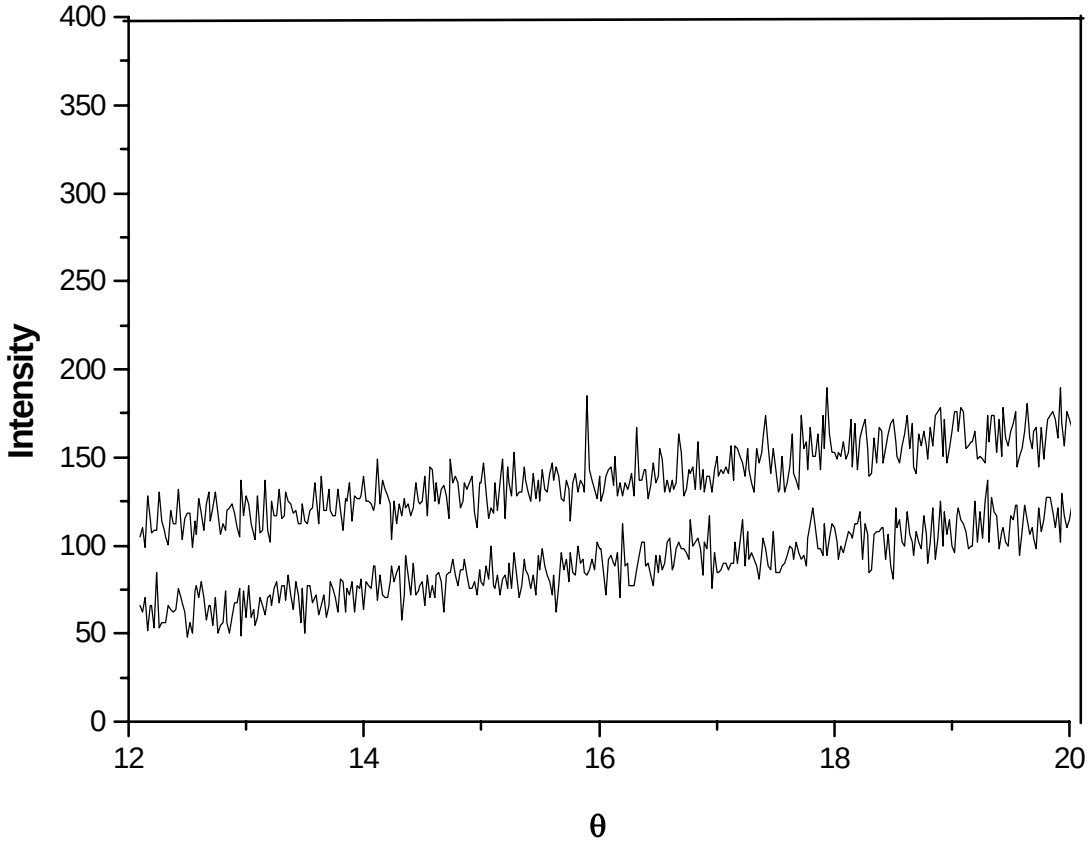

Figure 5.12 the rocking curve of NiSi (001) peak of the Group C sample (pure Ni) annealed at 500^{o}C and 600^{o}C

We found that texture property was also strongly affected by Ni/Si ratio of the as-deposited sample. In Figure 5.11, the rocking curve of Group B sample annealed at 500^{o}C gives 2 peaks, which means that Group B sample possessed two preferred orientations. The Group C sample annealed at different temperatures (seen in Figure 5.12) gives no peaks in Rocking curve results. The Rocking curve results are consistent with θ-2θ XRD results, and further confirms our earlier conclusion.

Conclusions

In summary, NiSi textured thin film can be well fabricated by Pulsed laser deposition with proper Ni/Si ratio. NiSi thin film prepared by Ni/Si target possessed the preferred orientation of NiSi (001) on Si (001) substrate. XRD and Rocking curve results prove that the texture properties of NiSi thin film are strongly affected by both Ni/Si ratio and annealing temperature.

5.4 References

[5.1] J. F. Liu, J. Y. Feng, and J. Zhu, *Appl. Phys. Lett.*, **80**, 14 (2002).

[5.2] J. F. Liu, H. B. Chen, J. Y. Feng, and J. Zhu, *Appl. Phys. Lett.*, **77**, 2 (2000).

[5.3] Gi Bum Kim, Do-Joon Yoo, Hong Koo Baik, and Jae-Min Myoung, *J. Vac. Sci. Technol. B*, **21**, 1 (2003).

.

[5.4] D. Mangelinck, J. Y. Dai, J. S. Pan, and S. K. Lahiri, *Appl. Phys. Lett.*, **75**, 20 (1999).

[5.5] A. S. W. Wong, D. Z. Chi, M. Loomans, D. Ma, M. Y. Lai, W. C. Tjiu, and S. J. Chua, *Appl. Phys. Lett.*, **81**, 30 (2002).

Chapter 6

Conclusions and future Work

Conclusions:

In this work, NiSi thin films were prepared by Pulsed Laser Deposition and studied using Raman spectroscopy and XRD. We have shown Raman spectroscopy to be a very powerful tool for Ni silicide phase identification. NiSi thin films can be reliably fabricated by Pulsed Laser Deposition with different Ni/Si ratio. The use of Ni and Si targets together was found to enhance the thin film surface smoothness.

NiSi thin films prepared with Ni/Si targets possessed the preferred orientation of NiSi (001) on Si (001) substrate. Texture properties of NiSi thin films are strongly affected by both Ni/Si ratio and annealing temperature, as shown by XRD and Rocking curve results.

Future work:

We successfully fabricated NiSi thin film of preferred orientation by PLD using Ni/Si target. Although the preferred orientation of NiSi (001) on Si (001) substrate is proved by XRD and rocking curve results, the mechanism of thin film preferred orientation formation is still not clear. Hence, further study on the mechanism of NiSi thin film preferred orientation formation would be interesting and promising.